Coupling modes in doubly odd nuclei: The case of ^{172}Ta

D. Hojman,[1,2,4] M. A. Cardona,[1,2] M. Davidson,[3,4] M. E. Debray,[1,2] A. J. Kreiner,[1,2,4] F. Le Blanc,[8] A. Burlon,[1] J. Davidson,[3,4] G. Levinton,[1] H. Somacal,[2] J. M. Kesque,[1] F. Naab,[1] M. Ozafrán,[1] P. Stoliar,[1] M. Vázquez,[1] D. R. Napoli,[5] D. Bazzacco,[6] N. Blasi,[7] S. M. Lenzi,[6] G. Lo Bianco,[7] and C. Rossi Alvarez[6]

[1]*Departamento de Física, Comisión Nacional de Energía Atómica, 1429 Buenos Aires, Argentina*

[2]*Escuela de Ciencia y Tecnología, Universidad de San Martín, San Martín, 1650 San Martín, Argentina*

[3]*Departamento de Física, Facultad de Ciencias Exactas y Naturales, Universidad de Buenos Aires, Buenos Aires, Argentina*

[4]*CONICET, 1033 Buenos Aires, Argentina*

[5]*INFN, Laboratori Nazionali di Legnaro, Legnaro, Italy*

[6]*Dipartimento di Fisica, Sezione di Padova, Padova, Italy*

[7]*Dipartimento di Fisica and INFN, Sezione di Milano, Milano, Italy*

[8]*Institut de Physique Nucléaire, IN2P3-CNRS, 91406 Orsay Cedex, France*

(Received 16 August 1999; published 22 May 2000)

High-spin states in doubly odd ^{172}Ta were investigated in two different experiments by means of in-beam γ-ray and internal-conversion electron spectroscopy techniques. Excited states of ^{172}Ta were populated using the ^{159}Tb(^{18}O,5n) and ^{165}Ho(^{12}C,5n) reactions at beam energies of 93 and 79 MeV, respectively. Eleven rotational bands, including twin bands in the normal deformation regime, have been observed and their configurations discussed. Three isomeric states have been found and their half-lives measured. Alignments, band crossing frequencies, and electromagnetic properties have been analyzed in the framework of the cranking model.

PACS number(s): 21.10.Re, 21.60.Ev, 23.20.Lv, 27.70.+q

I. INTRODUCTION

Doubly odd nuclei belonging to the deformed heavy rare-earth region have revealed a large number of interesting nuclear structure phenomena. Among them, the discovery [1] of the twin band phenomenon in the normal deformation regime stands out, comprising cases where the mechanism seems to be understood [1] and others where it is not yet clear [2,3]. In addition, signature inversion in $\pi h_{9/2} \otimes \nu i_{13/2}$ bands has been recently discovered in ^{162,164}Tm, ^{174}Ta, and ^{176}Re [4–6] and analyzed [6] in terms of the experimental proton-neutron force present in ^{208}Bi [7]. Particularly until the construction of high-efficiency multidetector arrays, the main experimental problem to identify the intrinsic structure of a given band was the difficulty to obtain information about the connection among the high spin bands of doubly odd nuclei populated by fusion-evaporation reactions using heavy ion beams and the known, usually lower spin parts of the level scheme and the determination of the spin and parity of the bandheads. To overcome this problem a general classification scheme for the coupling modes of two nonidentical valence nucleons [8–11] was developed. In this context, we reexamined [12] the doubly odd nucleus ^{172}Ta using the GASP multidetector array at the Legnaro Tandem Facility and the low energy spectroscopy facility at the Tandar Laboratory in Buenos Aires. We selected this doubly odd nucleus as an appropriate testing ground for the general classification scheme due to the large number of rotational bands expected near the yrast line.

II. EXPERIMENTS AND RESULTS

A. Measurements

In a first experiment high spin states of ^{172}Ta were populated through the ^{159}Tb(^{18}O,5n) fusion-evaporation reaction at 93 MeV. The target consisted of a 2 mg/cm^2 Tb foil, backed with a 2 mg/cm^2 evaporated Bi layer. The beam was provided by the Tandem XTU accelerator of Legnaro and γ rays emitted by the evaporation residues were detected using the GASP array [13], which consisted of 40 Compton suppressed large volume Ge detectors, and a multiplicity filter of 80 bismuth germanate (BGO) elements, providing the sum-energy and γ-ray multiplicity used to select the different reaction channels. Events were collected when at least three suppressed Ge and three inner multiplicity filter detectors were fired. With this condition a total of $\approx 4\times10^9$ events were recorded. With these data we constructed a fully symmetrized E_γ-E_γ-E_γ and an E_γ-E_γ-multiplicity cubes and an angular correlation matrix. The three known bands in ^{172}Ta [12] were extended up $\approx 6-7$ units of $\hbar$ and nine new bands were assigned to this nucleus, including the unfavored part of the $\pi h_{9/2} \otimes \nu 1/2^-[521]$ doubly decoupled band.

A second experiment was performed at the TANDAR Laboratory in Buenos Aires, in order to search for isomeric states and to determine the multipolarity of some transitions playing a special role in the deexcitation scheme. In this experiment ^{172}Ta was populated through the ^{165}Ho(^{12}C,5n) reaction at $E(^{12}\mathrm{C}) = 79$ MeV. The targets consisted of a 4 mg/cm^2 and a 500 μg/cm^2 Ho foil. The first one was used to determine the half-lives of the isomeric transitions and the second one to measure internal conversion coefficients (icc). A total of $\approx 8\times10^6$ and 80×10^6 events were respectively recorded. The experimental setup consisted of a high resolution Ge planar detector, an 11 NaI(Tl) element multiplicity filter and a Si(Li) electron detector coupled to a miniorange spectrometer. E_γ-t and E_e-t matrices were constructed, where the time was measured relative to the multiplicity filter which provided the stop signal in the coincidences.

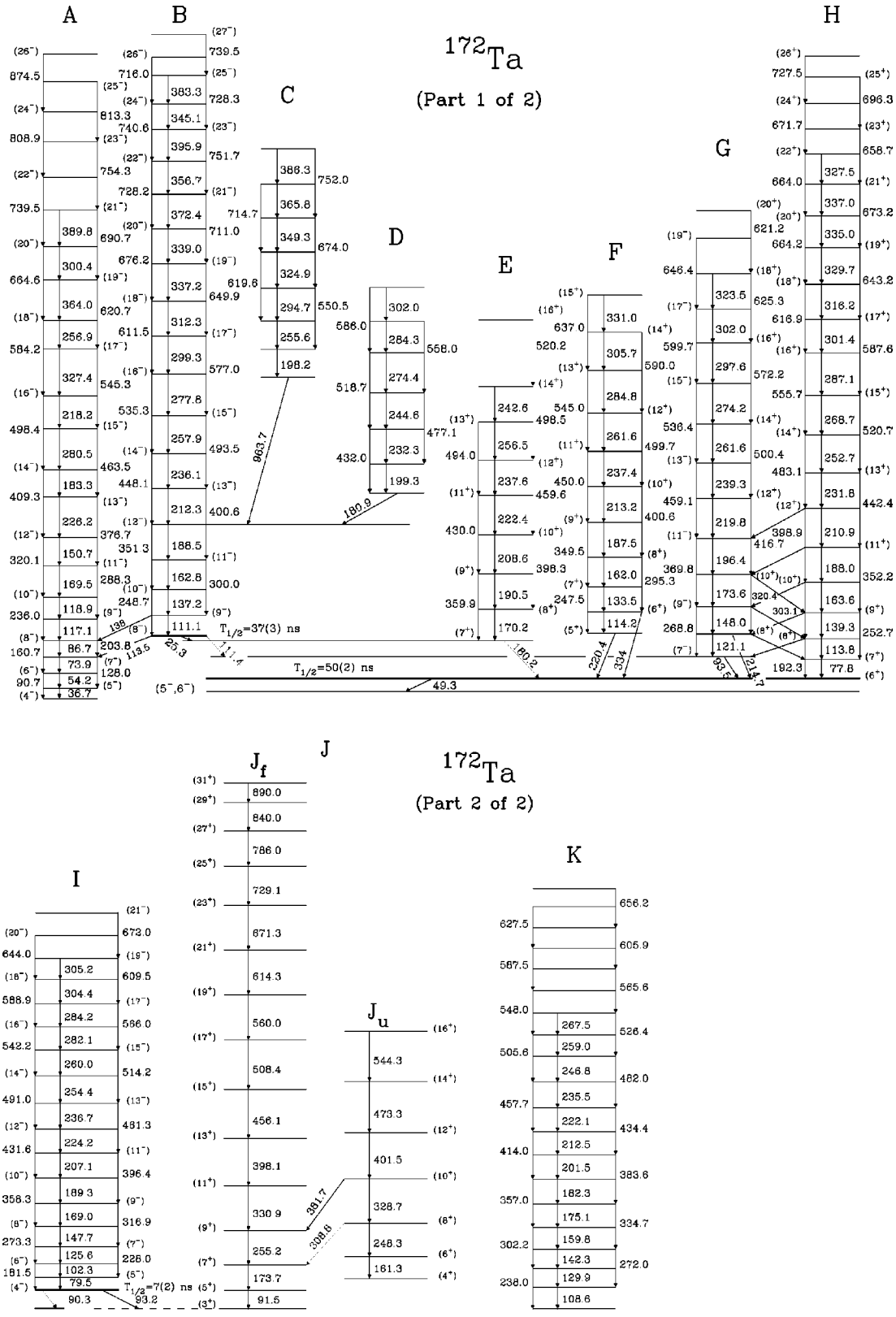

FIG. 1. Level scheme of ^{172}Ta proposed in the present work.

B. Level scheme

The level scheme of ^{172}Ta deduced in the present work is shown in Fig. 1. The assignment of transitions belonging to ^{172}Ta was based on multiplicity, which is well separated for channels differing in one evaporated neutron, coincidences with Ta x rays and other transitions assigned previously to this nucleus [12] and the knowledge of the neighboring odd Ta nuclei [14,15]. Figures 2, 3, and 4 show summed coinci-

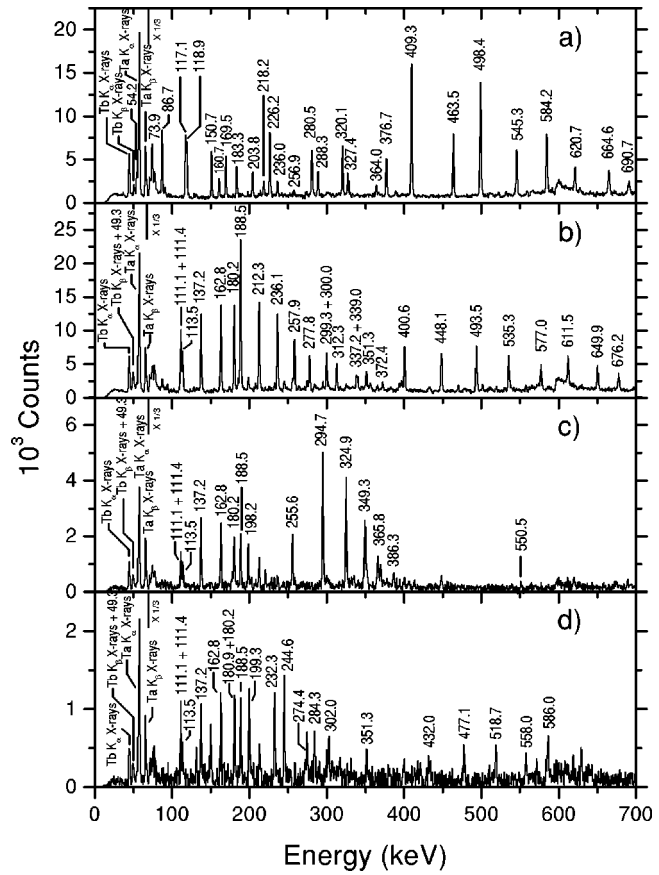

FIG. 2. γ-ray coincidence spectra of Ge detectors corresponding to the sum of several gates on pairs of transitions belonging to the same band: (a) band A, (b) band B, (c) band C, and (d) band D.

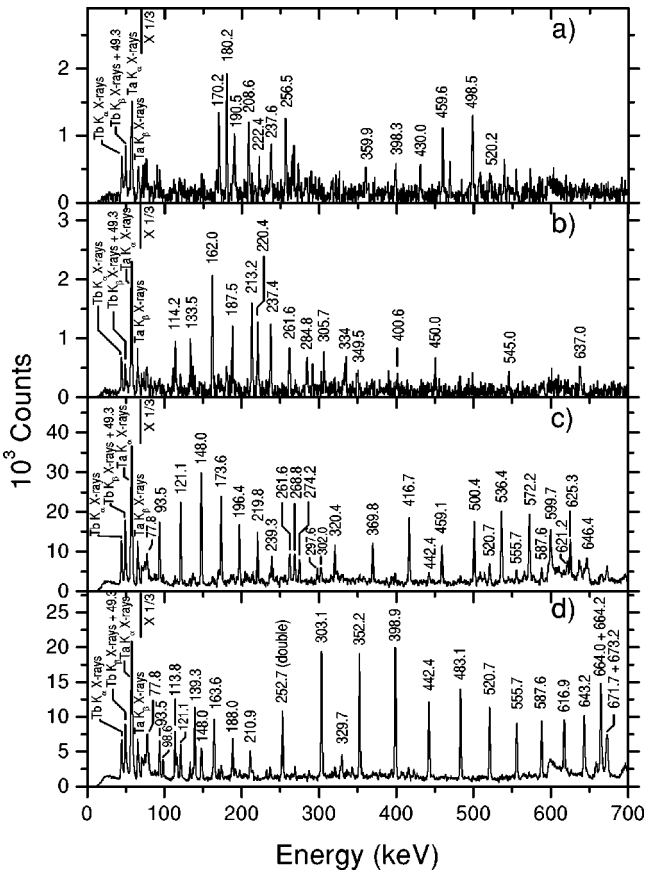

FIG. 3. γ-ray coincidence spectra of Ge detectors corresponding to the sum of several gates on pairs of transitions belonging to the same band: (a) band E, (b) band F, (c) band G, and (d) band H.

dence spectra, for bands from A to K, gated on pairs of transitions belonging to the same band. Figure 5 shows a delayed electron spectrum, from 60 to 120 ns. Bands can be classified, according to their intensity, in strongly populated bands (A, B, H, and J_f), weakly populated bands (C, D, E, F, and J_u) and bands in an intermediate situation (G, I, and K). γ-ray intensities cannot be accurately obtained because of the complexity of the singles and projection spectra. Moreover, pure γ-rays are almost always only observed in double gated spectra.

Transition energies, spin assignments, branching ratios, DCO ratios (directional correlations of γ rays deexciting oriented states) and the evaluated $B(M1)/B(E2)$ ratios are listed in Table I grouped in sequences for each band or pairs of linked bands. The experimental branching ratio for a given state was obtained from relative γ-ray intensity in the spectrum in coincidence with two transitions directly populating that state. The DCO calculations have been carried out for $\theta_1 = 34.6°(145.4°)$, $\theta_2 = 90°$, and $\langle\phi\rangle = 69.7°$ ($\langle\phi\rangle$ is the average relative angular position of the detectors at θ_1 and θ_2 in the GASP geometry). In the GASP geometry, setting gates on stretched quadrupole transitions, leads to theoretical DCO ratios $I\gamma_{\text{gate}=\theta_2}(\theta_1)/I\gamma_{\text{gate}=\theta_1}(\theta_2) \approx 1$ for stretched quadrupole transitions and ≈ 0.6 for pure dipole ones. The experimental $B(M1)/B(E2)$ ratios were determined by the following expression:

$$\frac{B(M1,I\rightarrow I-1)}{B(E2,I\rightarrow I-2)} = 0.697 \frac{E_{\gamma_2}^5}{E_{\gamma_1}^3} \frac{1}{\lambda(1+\delta^2)} \left[\frac{\mu_N^2}{(e\,b)^2}\right],$$

where E_{γ_1,γ_2} are the energies (in MeV) corresponding to the $\Delta I = 1,2$ transitions, respectively, λ the γ-ray intensity ratio $I(\gamma_2)/I(\gamma_1)$, and δ the mixing ratio of the $\Delta I = 1$ transition. For the $B(M1)/B(E2)$ ratios reported in Table I we assumed $\delta^2 = 0$ (for $|\delta| < 0.3$ the errors produced with this assumption are less than 10%). Table II reports icc extracted from intensity balances, using double gated spectra, for transitions playing a special role in the level scheme.

Figure 6 shows the spectra measured with the high resolution planar detector in different time conditions. Only relevant transitions are labeled. In particular in the spectra gated with the time condition 200 ns $< T <$ 350 ns [Fig. 6(e)] we can clearly see the 35.7 keV and 130.2 keV $E1$ transitions belonging to ^{173}Ta, reported by Kurniawan and co-workers [16] in the depopulation of a state with $T_{1/2} = 225(15)$ ns. In order to obtain the values of the half-lives involved in delayed transitions, we have fitted the time spectra using an exponential decay folded with the prompt spectrum extracted from the 117.1 keV line (assigned to band A of ^{172}Ta). The half-life $T_{1/2} = 89.3(10)$ ns reported for the state depopulated through the 197.1 keV line in ^{19}F [17] has been used as a

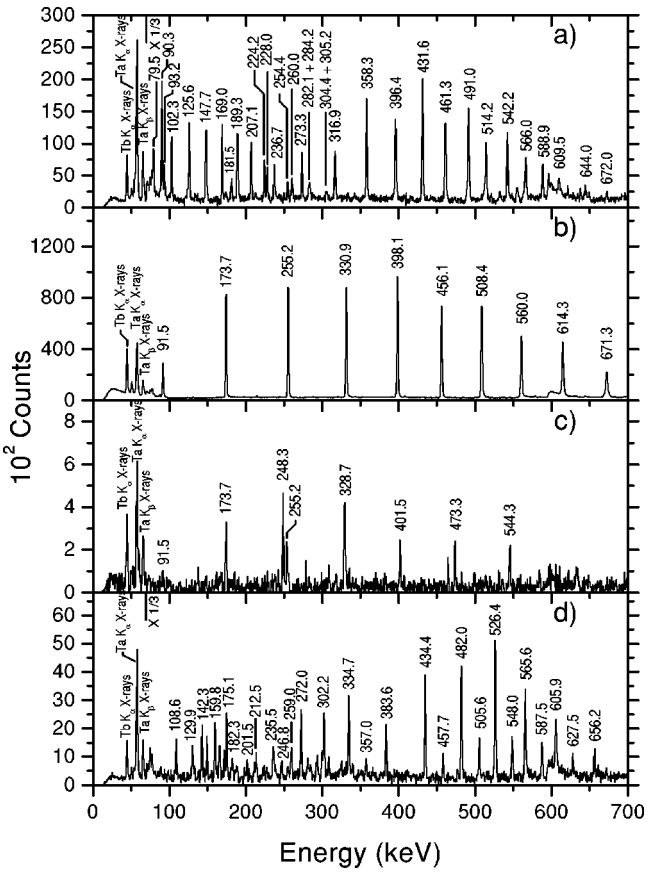

FIG. 4. γ-ray coincidence spectra of Ge detectors corresponding to the sum of several gates on pairs of transitions belonging to the same band: (a) band I, (b) band J (favored), (c) band J (unfavored), and (d) band K.

test, obtaining in our case $T_{1/2}=89(2)$ ns. Figure 7 shows time spectra gated on the 117.1 keV (prompt), 90.3 keV, 180.2 keV, and 49.3 keV lines. The values obtained for these delayed transitions are $T_{1/2}=7(2)$, 37(3), and 50(2) ns, respectively. For the 49.3 keV line the fit was performed using two exponential decays because of the involved isomeric state is populated mainly through the delayed 25.3 and 180.2 keV transitions.

Bands A, H, and J_f have been reported in a previous work [12]. Band A has been extended up to $26\hbar$ and three new $\Delta I=1$ low-energy transitions, with the corresponding crossover transitions, placed in its low-lying region. The previous spin assignment [12] has been changed in three units because of the new observed states and the signature inversion observed in this work (see discussion). This band is connected with band B through the 113.5 and 138 keV transitions. The $M1(E2)$ character of the 113.5 keV line, deduced from intensity balance and icc (see Tables II and III) fixes unambiguously the parity of band B because of the negative parity of band A (see discussion). Band B is observed up to $27\hbar$. This band depopulates, in addition to band A, from its bandhead to bands E and G through the 25.3 and 111.4 keV transitions, respectively. The $E1$ character of these transitions comes from intensity balance (see Table II) and fixes the parity (positive) of bands E, F, G, and H, taking into account the connections among them. Bands C and D depopulate to the (12^-) state of band B through the 963.7 and 180.9 keV transitions. The weak intensity of these bands does not allow us to determine the multipolarity of the linking transitions (through DCO ratios or intensity balance) and to fix spin and parity of the bands. Bands E and F, observed up to $16\hbar$ and $15\hbar$, respectively, depopulate to the head of band H, through the 180.2, 220.4, and 334 keV lines. The $M1$ character (with $E2$ mixing) of the first two transitions comes from intensity balances (see Table II) and, for the 180.2 keV transition, from measured icc (see Table III). Bands G and H, observed up to $20\hbar$ and $26\hbar$, respectively, show multiple linking transitions fixing unambiguously their relative spins. The H bandhead deexcites through a 49.3 keV isomeric transition to a negative parity state with spin $I=5$ or 6. This value has been restricted from rotational argu-

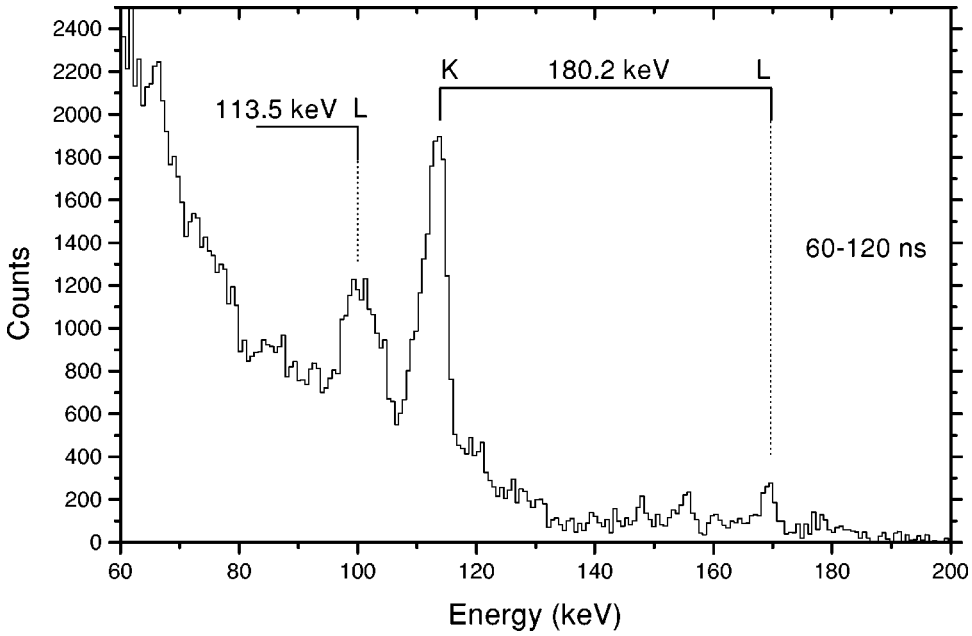

FIG. 5. Delayed electron spectrum (see text).

TABLE I. γ-ray transition energies, spin assignments, branching ratios, DCO ratios, and $B(M1)/B(E2)$ ratios in ^{172}Ta.

E_γ (keV)[a]	$I_i^\pi \rightarrow I_f^\pi$	Branching ratio[b]	DCO ratio[c]	$B(M1)/B(E2)$[d] $(\mu_N^2/e^2\,b^2)$
Band A				
36.7	$(5^-)\rightarrow(4^-)$			
54.2	$(6^-)\rightarrow(5^-)$			
73.9	$(7^-)\rightarrow(6^-)$	0.13(3)		0.46(12)
86.7	$(8^-)\rightarrow(7^-)$	0.28(6)		0.42(8)
90.7	$(6^-)\rightarrow(4^-)$			
117.1	$(9^-)\rightarrow(8^-)$	0.55(9)	0.59(4)	0.27(4)
118.9	$(10^-)\rightarrow(9^-)$	0.98(15)	0.59(3)	0.31(5)
128.0	$(7^-)\rightarrow(5^-)$			
150.7	$(12^-)\rightarrow(11^-)$	3.01(5)	0.51(6)	0.23(4)
160.7	$(8^-)\rightarrow(6^-)$		1.05(13)	
169.5	$(11^-)\rightarrow(10^-)$	1.09(16)	0.41(2)	0.26(4)
183.3	$(14^-)\rightarrow(13^-)$	5.27(84)	0.46(7)	0.25(4)
203.8	$(9^-)\rightarrow(7^-)$		0.98(5)	
218.2	$(16^-)\rightarrow(15^-)$	12.3(20)	0.46(5)	0.17(3)
226.2	$(13^-)\rightarrow(12^-)$	1.73(22)	0.39(3)	0.26(3)
236.0	$(10^-)\rightarrow(8^-)$		1.00(3)	
256.9	$(18^-)\rightarrow(17^-)$			
280.5	$(15^-)\rightarrow(14^-)$	2.35(32)	0.50(15)	0.29(4)
288.3	$(11^-)\rightarrow(9^-)$		0.99(7)	
300.4	$(20^-)\rightarrow(19^-)$			
320.1	$(12^-)\rightarrow(10^-)$		1.11(9)	
327.4	$(17^-)\rightarrow(16^-)$		0.42(6)	
364.0	$(19^-)\rightarrow(18^-)$			
376.7	$(13^-)\rightarrow(11^-)$		1.01(10)	
389.8	$(21^-)\rightarrow(20^-)$			
409.3	$(14^-)\rightarrow(12^-)$		1.05(7)	
463.5	$(15^-)\rightarrow(13^-)$		1.05(5)	
498.4	$(16^-)\rightarrow(14^-)$		1.02(10)	
545.3	$(17^-)\rightarrow(15^-)$		1.04(3)	
584.2	$(18^-)\rightarrow(16^-)$		1.00(8)	
620.7	$(19^-)\rightarrow(17^-)$		0.96(8)	
664.6	$(20^-)\rightarrow(18^-)$		0.97(8)	
690.7	$(21^-)\rightarrow(19^-)$		0.89(6)	
739.5	$(22^-)\rightarrow(20^-)$		0.89(9)	
754.3	$(23^-)\rightarrow(21^-)$		0.91(11)	
808.9	$(24^-)\rightarrow(22^-)$		0.83(2)	
813.3	$(25^-)\rightarrow(23^-)$			
874.5	$(26^-)\rightarrow(24^-)$			
Band B				
111.1	$(9^-)\rightarrow(8^-)$		1.30(14)	
137.2	$(10^-)\rightarrow(9^-)$	0.05(1)	1.13(14)	4.77(100)
162.8	$(11^-)\rightarrow(10^-)$	0.42(6)	0.98(6)	0.94(13)
188.5	$(12^-)\rightarrow(11^-)$	0.40(6)	0.95(6)	1.40(21)
212.3	$(13^-)\rightarrow(12^-)$	0.64(10)	0.88(5)	1.16(19)
236.1	$(14^-)\rightarrow(13^-)$	0.81(11)	0.81(5)	1.18(17)
248.7	$(10^-)\rightarrow(8^-)$			
257.9	$(15^-)\rightarrow(14^-)$	1.15(17)	0.81(14)	1.01(15)
277.8	$(16^-)\rightarrow(15^-)$	1.06(21)	0.76(8)	1.33(27)
299.3	$(17^-)\rightarrow(16^-)$	1.32(22)	0.93(10)	1.26(21)
300.0	$(11^-)\rightarrow(9^-)$		0.93(10)	

TABLE I. (*Continued*).

E_γ (keV)[a]	$I_i^\pi \rightarrow I_f^\pi$	Branching ratio[b]	DCO ratio[c]	$B(M1)/B(E2)$[d] ($\mu_N^2/e^2\,\mathrm{b}^2$)
312.3	$(18^-)\rightarrow(17^-)$	1.80(32)	0.71(13)	1.08(19)
337.2	$(19^-)\rightarrow(18^-)$	2.46(52)	0.65(9)	0.86(18)
339.0	$(20^-)\rightarrow(19^-)$		0.66(9)	
345.1	$(24^-)\rightarrow(23^-)$			
351.3	$(12^-)\rightarrow(10^-)$		1.15(20)	
356.7	$(22^-)\rightarrow(21^-)$		0.68(7)	
372.4	$(21^-)\rightarrow(20^-)$		1.19(12)	
383.3	$(25^-)\rightarrow(24^-)$			
395.9	$(23^-)\rightarrow(22^-)$			
400.6	$(13^-)\rightarrow(11^-)$		1.19(18)	
448.1	$(14^-)\rightarrow(12^-)$	1.06(10)		
493.5	$(15^-)\rightarrow(13^-)$		1.07(18)	
535.3	$(16^-)\rightarrow(14^-)$		1.14(22)	
577.0	$(17^-)\rightarrow(15^-)$		0.98(7)	
611.5	$(18^-)\rightarrow(16^-)$		1.00(11)	
649.9	$(19^-)\rightarrow(17^-)$		1.02(7)	
676.2	$(20^-)\rightarrow(18^-)$		1.03(9)	
711.0	$(21^-)\rightarrow(19^-)$		1.03(14)	
716.0	$(26^-)\rightarrow(24^-)$			
728.2	$(22^-)\rightarrow(20^-)$		1.00(17)	
728.3	$(25^-)\rightarrow(23^-)$			
739.5	$(27^-)\rightarrow(25^-)$			
740.6	$(24^-)\rightarrow(22^-)$			
751.7	$(23^-)\rightarrow(21^-)$		1.03(15)	
Band C				
198.2				
255.6				
294.7		0.17(4)		0.94(19)
324.9		0.35(7)		5.2(11)
349.3		0.44(9)		5.2(10)
365.8				
386.3				
550.5				
619.6				
674.0				
714.7				
752.0				
Band D				
199.3				
232.3		0.66(15)		1.26(29)
244.6		0.86(15)		1.37(25)
274.4		1.48(27)		0.85(15)
284.3		1.06(19)		1.54(28)
302.0				
432.0				
477.1				
518.7				
558.0				
586.0				
Band E				
170.2	$(8^+)\rightarrow(7^+)$			
190.5	$(9^+)\rightarrow(8^+)$	0.66(11)	1.06(11)	0.91(22)

TABLE I. (*Continued*).

E_γ (keV)[a]	$I_i^\pi \rightarrow I_f^\pi$	Branching ratio[b]	DCO ratio[c]	$B(M1)/B(E2)$[d] $(\mu_N^2/e^2\,\mathrm{b}^2)$
208.6	$(10^+)\rightarrow(9^+)$	0.97(19)	0.84(16)	0.81(16)
222.4	$(11^+)\rightarrow(10^+)$	1.08(22)		0.70(14)
237.6	$(12^+)\rightarrow(11^+)$	1.93(37)		0.55(10)
242.6	$(14^+)\rightarrow(13^+)$			
256.5	$(13^+)\rightarrow(12^+)$		0.78(8)	
359.9	$(9^+)\rightarrow(7^+)$			
398.3	$(10^+)\rightarrow(8^+)$		1.21(12)	
430.0	$(11^+)\rightarrow(9^+)$		1.03(10)	
459.6	$(12^+)\rightarrow(10^+)$		0.93(5)	
494.0	$(13^+)\rightarrow(11^+)$			
498.5	$(14^+)\rightarrow(12^+)$		1.10(11)	
520.2	$(16^+)\rightarrow(14^+)$			
Band F				
114.2	$(6^+)\rightarrow(5^+)$			
133.5	$(7^+)\rightarrow(6^+)$			
162.0	$(8^+)\rightarrow(7^+)$		1.07(16)	
187.5	$(9^+)\rightarrow(8^+)$		1.31(22)	
213.2	$(10^+)\rightarrow(9^+)$			
237.4	$(11^+)\rightarrow(10^+)$			
247.5	$(7^+)\rightarrow(5^+)$			
261.6	$(12^+)\rightarrow(11^+)$			
284.8	$(13^+)\rightarrow(12^+)$			
295.3	$(8^+)\rightarrow(6^+)$			
305.7	$(14^+)\rightarrow(13^+)$			
331.0	$(15^+)\rightarrow(14^+)$			
349.5	$(9^+)\rightarrow(7^+)$			
400.6	$(10^+)\rightarrow(8^+)$			
450.0	$(11^+)\rightarrow(9^+)$			
499.7	$(12^+)\rightarrow(10^+)$			
545.0	$(13^+)\rightarrow(11^+)$			
590.0	$(14^+)\rightarrow(12^+)$			
637.0	$(15^+)\rightarrow(13^+)$			
Band G				
121.1	$(8^+)\rightarrow(7^+)$		1.18(17)	
148.0	$(9^+)\rightarrow(8^+)$	0.48(10)	1.08(23)	0.62(12)
173.6	$(10^+)\rightarrow(9^+)$	0.89(14)	1.22(20)	0.50(8)
196.4	$(11^+)\rightarrow(10^+)$	1.50(23)	1.09(13)	0.42(6)
219.8	$(12^+)\rightarrow(11^+)$	2.45(37)	0.98(19)	0.34(5)
239.3	$(13^+)\rightarrow(12^+)$	2.30(53)	0.92(10)	0.45(10)
261.6	$(14^+)\rightarrow(13^+)$	4.10(70)	0.80(6)	0.30(5)
268.8	$(9^+)\rightarrow(7^+)$		0.76(13)	
274.2	$(15^+)\rightarrow(14^+)$	5.5(11)	0.67(7)	0.27(5)
297.6	$(16^+)\rightarrow(15^+)$		0.65(7)	
302.0	$(17^+)\rightarrow(16^+)$		0.85(14)	
320.4	$(10^+)\rightarrow(8^+)$		1.14(7)	
323.5	$(18^+)\rightarrow(17^+)$			
369.8	$(11^+)\rightarrow(9^+)$		1.05(14)	
416.7	$(12^+)\rightarrow(10^+)$		0.90(10)	
459.1	$(13^+)\rightarrow(11^+)$		0.99(10)	
500.4	$(14^+)\rightarrow(12^+)$		0.99(10)	
536.4	$(15^+)\rightarrow(13^+)$		1.09(7)	
572.2	$(16^+)\rightarrow(14^+)$		1.09(16)	

TABLE I (*Continued*).

E_γ (keV)[a]	$I_i^\pi \rightarrow I_f^\pi$	Branching ratio[b]	DCO ratio[c]	$B(M1)/B(E2)$[d] $(\mu_N^2/e^2\,\mathrm{b}^2)$
599.7	$(17^+)\rightarrow(15^+)$		0.82(9)	
621.2	$(20^+)\rightarrow(18^+)$		1.04(7)	
625.3	$(18^+)\rightarrow(16^+)$		1.04(3)	
646.4	$(19^+)\rightarrow(17^+)$		1.01(10)	
Band H				
77.8	$(7^+)\rightarrow(6^+)$		1.29(9)	
113.8	$(8^+)\rightarrow(7^+)$	0.33(7)	1.94(32)	0.37(7)
139.3	$(9^+)\rightarrow(8^+)$	0.92(19)	1.51(22)	0.29(6)
163.6	$(10^+)\rightarrow(9^+)$	2.56(38)	1.22(10)	0.16(2)
188.0	$(11^+)\rightarrow(10^+)$	6.39(96)	1.27(7)	0.09(1)
192.3	$(8^+)\rightarrow(6^+)$			
210.9	$(12^+)\rightarrow(11^+)$	5.2(10)	1.00(6)	0.14(3)
231.8	$(13^+)\rightarrow(12^+)$	7.9(11)	0.98(11)	0.12(2)
252.7	$(9^+)\rightarrow(7^+)$			
252.7	$(14^+)\rightarrow(13^+)$			
268.7	$(15^+)\rightarrow(14^+)$	8.6(14)	0.92(9)	0.16(3)
287.1	$(16^+)\rightarrow(15^+)$	9.0(15)	0.94(9)	0.17(3)
301.4	$(17^+)\rightarrow(16^+)$	12.6(25)		0.14(3)
303.1	$(10^+)\rightarrow(8^+)$		1.02(9)	
316.2	$(18^+)\rightarrow(17^+)$	14.5(31)	1.07(23)	0.14(3)
327.5	$(22^+)\rightarrow(21^+)$			
329.7	$(19^+)\rightarrow(18^+)$		0.96(5)	
335.0	$(20^+)\rightarrow(19^+)$			
337.0	$(21^+)\rightarrow(20^+)$			
352.2	$(11^+)\rightarrow(9^+)$		1.15(21)	
398.9	$(12^+)\rightarrow(10^+)$		1.12(10)	
442.4	$(13^+)\rightarrow(11^+)$		1.07(6)	
483.1	$(14^+)\rightarrow(12^+)$		1.13(13)	
520.7	$(15^+)\rightarrow(13^+)$		1.03(10)	
555.7	$(16^+)\rightarrow(14^+)$		1.04(5)	
587.6	$(17^+)\rightarrow(15^+)$		1.05(10)	
616.9	$(18^+)\rightarrow(16^+)$		0.96(5)	
643.2	$(19^+)\rightarrow(17^+)$		0.93(5)	
658.7	$(23^+)\rightarrow(21^+)$		0.97(7)	
664.0	$(22^+)\rightarrow(20^+)$			
664.2	$(20^+)\rightarrow(18^+)$		1.02(17)	
671.7	$(24^+)\rightarrow(22^+)$			
673.2	$(21^+)\rightarrow(19^+)$			
696.3	$(25^+)\rightarrow(23^+)$			
727.5	$(26^+)\rightarrow(24^+)$			
Band I				
79.5	$(5^-)\rightarrow(4^-)$			
102.3	$(6^-)\rightarrow(5^-)$	0.50(9)	0.86(10)	0.26(5)
125.6	$(7^-)\rightarrow(6^-)$	0.78(13)	0.63(10)	0.28(5)
147.7	$(8^-)\rightarrow(7^-)$	1.15(18)	0.75(12)	0.29(4)
169.0	$(9^-)\rightarrow(8^-)$	1.64(27)		0.28(4)
181.5	$(6^-)\rightarrow(4^-)$		0.89(11)	
189.3	$(10^-)\rightarrow(9^-)$	2.39(41)	0.79(6)	0.25(4)
207.1	$(11^-)\rightarrow(10^-)$	2.77(50)		0.28(5)
224.2	$(12^-)\rightarrow(11^-)$	3.73(59)		0.25(4)
228.0	$(7^-)\rightarrow(5^-)$		0.87(6)	
236.7	$(13^-)\rightarrow(12^-)$	3.80(68)		0.29(5)

TABLE I. (*Continued*).

E_γ (keV)[a]	$I_i^\pi \rightarrow I_f^\pi$	Branching ratio[b]	DCO ratio[c]	$B(M1)/B(E2)$[d] $(\mu_N^2/e^2\,\mathrm{b}^2)$
254.4	$(14^-)\rightarrow(13^-)$	4.08(77)		0.30(5)
260.0	$(15^-)\rightarrow(14^-)$			
273.3	$(8^-)\rightarrow(6^-)$		0.95(5)	
282.1	$(16^-)\rightarrow(15^-)$			
284.2	$(17^-)\rightarrow(16^-)$			
304.4	$(18^-)\rightarrow(17^-)$			
305.2	$(19^-)\rightarrow(18^-)$			
316.9	$(9^-)\rightarrow(7^-)$		1.00(3)	
358.3	$(10^-)\rightarrow(8^-)$		1.04(12)	
396.4	$(11^-)\rightarrow(9^-)$		0.98(5)	
431.6	$(12^-)\rightarrow(10^-)$		1.03(16)	
461.3	$(13^-)\rightarrow(11^-)$		0.97(8)	
491.0	$(14^-)\rightarrow(12^-)$		1.08(6)	
514.2	$(15^-)\rightarrow(13^-)$		0.98(6)	
542.2	$(16^-)\rightarrow(14^-)$		1.12(16)	
566.0	$(17^-)\rightarrow(15^-)$		1.03(8)	
588.9	$(18^-)\rightarrow(16^-)$		1.17(7)	
609.5	$(19^-)\rightarrow(17^-)$			
644.0	$(20^-)\rightarrow(18^-)$			
672.0	$(21^-)\rightarrow(19^-)$			
Band J				
favored band (f)				
91.5	$(5^+)\rightarrow(3^+)$		1.68(21)	
173.7	$(7^+)\rightarrow(5^+)$		1.21(8)	
255.2	$(9^+)\rightarrow(7^+)$		0.99(5)	
330.9	$(11^+)\rightarrow(9^+)$		1.00(8)	
398.1	$(13^+)\rightarrow(11^+)$		0.96(8)	
456.1	$(15^+)\rightarrow(13^+)$		0.93(5)	
508.4	$(17^+)\rightarrow(15^+)$		0.97(5)	
560.0	$(19^+)\rightarrow(17^+)$		0.96(6)	
614.3	$(21^+)\rightarrow(19^+)$		0.90(8)	
671.3	$(23^+)\rightarrow(21^+)$		0.86(7)	
729.1	$(25^+)\rightarrow(23^+)$		0.90(11)	
786.0	$(27^+)\rightarrow(25^+)$			
840.0	$(29^+)\rightarrow(27^+)$			
890.0	$(31^+)\rightarrow(29^+)$			
unfavored band (u)				
161.3	$(6^+)\rightarrow(4^+)$		1.91(19)	
248.3	$(8^+)\rightarrow(6^+)$		0.96(4)	
328.7	$(10^+)\rightarrow(8^+)$		0.86(6)	
401.5	$(12^+)\rightarrow(10^+)$		0.99(7)	
473.3	$(14^+)\rightarrow(12^+)$		1.05(11)	
544.3	$(16^+)\rightarrow(14^+)$		1.43(3)	
Transitions	from u to f			
308.8	$(8^+)\rightarrow(7^+)$			
381.7	$(10^+)\rightarrow(9^+)$			
Band K				
108.6	$(K+1)\rightarrow(K)$			
129.9	$(K+2)\rightarrow(K+1)$	0.42(10)		0.58(14)
142.3	$(K+3)\rightarrow(K+2)$	1.27(24)	0.95(4)	0.28(5)
159.8	$(K+4)\rightarrow(K+3)$	1.07(18)	1.17(10)	0.40(7)
175.1	$(K+5)\rightarrow(K+4)$	2.15(34)	1.29(34)	0.25(4)

TABLE I. (*Continued*).

E_γ (keV)[a]	$I_i^\pi \rightarrow I_f^\pi$	Branching ratio[b]	DCO ratio[c]	$B(M1)/B(E2)$[d] $(\mu_N^2/e^2\,\mathrm{b}^2)$
182.3	$(K+6)\rightarrow(K+5)$	2.09(38)	0.81(15)	0.32(6)
201.5	$(K+7)\rightarrow(K+6)$	2.96(50)	0.85(10)	0.24(4)
212.5	$(K+8)\rightarrow(K+7)$	3.06(52)	1.10(15)	0.29(5)
222.1	$(K+9)\rightarrow(K+8)$	4.37(70)	0.74(10)	0.22(4)
235.5	$(K+10)\rightarrow(K+9)$	3.05(58)	1.04(10)	0.35(7)
238.0	$(K+2)\rightarrow(K)$			
246.8	$(K+11)\rightarrow(K+10)$	6.6(13)	0.80(6)	0.18(3)
259.0	$(K+12)\rightarrow(K+11)$	2.87(66)	0.85(10)	0.46(11)
267.5	$(K+13)\rightarrow(K+12)$			
272.0	$(K+3)\rightarrow(K+1)$		1.16(17)	
302.2	$(K+4)\rightarrow(K+2)$		0.96(4)	
334.7	$(K+5)\rightarrow(K+3)$		0.96(9)	
357.0	$(K+6)\rightarrow(K+4)$		1.00(10)	
383.6	$(K+7)\rightarrow(K+5)$		0.88(4)	
414.0	$(K+8)\rightarrow(K+6)$		1.14(10)	
434.4	$(K+9)\rightarrow(K+7)$		1.06(11)	
457.7	$(K+10)\rightarrow(K+8)$		1.11(25)	
482.0	$(K+11)\rightarrow(K+9)$		1.11(6)	
505.6	$(K+12)\rightarrow(K+10)$		1.05(9)	
526.4	$(K+13)\rightarrow(K+11)$		1.13(15)	
548.0	$(K+14)\rightarrow(K+12)$		1.18(20)	
565.6	$(K+15)\rightarrow(K+13)$		0.97(13)	
587.5	$(K+16)\rightarrow(K+14)$		1.05(10)	
605.9	$(K+17)\rightarrow(K+15)$		0.86(10)	
627.5	$(K+18)\rightarrow(K+16)$		1.53(25)	
656.2	$(K+19)\rightarrow(K+17)$			
Transitions	from B to A			
113.5	$(8^-)\rightarrow(7^-)$			
138	$(9^-)\rightarrow(8^-)$			
Transitions	from B to E			
25.3	$(8^-)\rightarrow(7^+)$			
Transitions	from B to G			
111.4	$(8^-)\rightarrow(7^+)$			
Transitions	from C to B			
963.7				
Transitions	from D to B			
180.9				
Transitions	from E to H			
180.2	$(7^+)\rightarrow(6^+)$			
Transitions	from F to H			
220.4	$(5^+)\rightarrow(6^+)$			
334	$(6^+)\rightarrow(6^+)$			
Transitions	from G to H			
93.5	$(7^+)\rightarrow(6^+)$			
136.5	$(8^+)\rightarrow(7^+)$			
170.5	$(9^+)\rightarrow(8^+)$			
203.7	$(10^+)\rightarrow(9^+)$			
214.7	$(8^+)\rightarrow(6^+)$			
Transitions	from H to G			
98.6	$(8^+)\rightarrow(7^+)$			
116.3	$(9^+)\rightarrow(8^+)$			
131.7	$(10^+)\rightarrow(9^+)$			

TABLE I. (*Continued*).

E_γ (keV)[a]	$I_i^\pi \rightarrow I_f^\pi$	Branching ratio[b]	DCO ratio[c]	$B(M1)/B(E2)$[d] $(\mu_N^2/e^2\,\mathrm{b}^2)$
147.3	$(11^+)\rightarrow(10^+)$			
159.3	$(12^+)\rightarrow(11^+)$			
Other transitions				
49.3	$(6^+)\rightarrow(5^-,6^-)$			
90.3				
93.2	$(4^-)\rightarrow(3^+)$			

[a]Uncertainties between 0.1 and 0.3 keV.
[b]Branching ratio: $I\gamma(I\rightarrow I-2)/I\gamma(I\rightarrow I-1)$, $I\gamma(I\rightarrow I-2)$, and $I\gamma(I\rightarrow I-1)$ are the relative γ intensities of the $\Delta I=2$ and $\Delta I=1$ transitions depopulating the spin I level, respectively.
[c]Directional correlation ratio: $I\gamma_{gate=\theta_2}(\theta_1)/I\gamma_{gate=\theta_1}(\theta_2)$ ($\theta_1=31.7°$, 36°, 144°, and 148.3° and $\theta_2=90°$) determined from coincidence spectra, setting gates on stretched $E2$ transitions on both axes of the DCO matrix.
[d]Determined assuming $\delta^2=0$.

TABLE II. Extracted internal conversion coefficients from intensity balances.

Double gate	γ ray	I_γ (arb. units)	Multipolarity	α	Assigned multipolarity
111.1–137.2	73.9	388(58)	$M1(E2)$		
	113.5	1091(109)		$2.37 \leqslant \alpha \leqslant 5.66$	$M1(E2)$
	128.0	93(28)	$E2$		
190.5–430.0	170.2	765(115)	$M1(E2)$		
	180.2	704(106)		$0.22 \leqslant \alpha \leqslant 1.93$	$M1(E2)$
111.1–137.2	25.3	1175(353)		$1.64 \leqslant \alpha \leqslant 6.73$	$E1$
	180.2	3136(314)	$M1(E2)$		
137.2–162.8	93.5	255(38)	$M1(E2)$		
	111.1	⎫	$M1(E2)$		
		6206(621)[a]			
	111.4	⎭		$\alpha \leqslant 1.68$	$E1$
	113.5	2122(212)	$M1(E2)$		
	180.2	4728(473)	$M1(E2)$		
133.5–162.0	114.2	135(20)	$M1(E2)$		
	220.4	262(26)		$0.30 \leqslant \alpha \leqslant 1.67$	$M1(E2)$
121.1–148.0	49.3	2139(535)		$0.43 \leqslant \alpha \leqslant 2.18$	$E1$
	93.5	720(72)	$M1(E2)$		
125.6–316.9	90.3	810(81)		$\alpha \leqslant 0.98$	$E1$
	93.2	271(27)		$\alpha \leqslant 1.95$	$E1$
	102.3	280(28)	$M1(E2)$		
	181.5	117(23)	$E2$		

[a]The intensity corresponds to the unresolved doublet 111.1 and 111.4 keV lines.

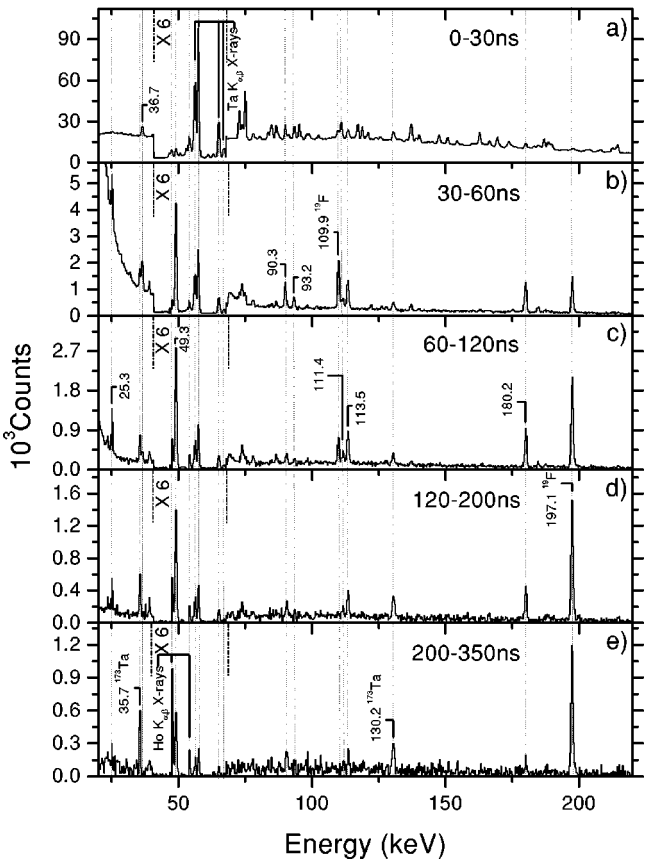

FIG. 6. High resolution γ-ray spectra with different time conditions (indicated in each plot). Only relevant transitions are labeled.

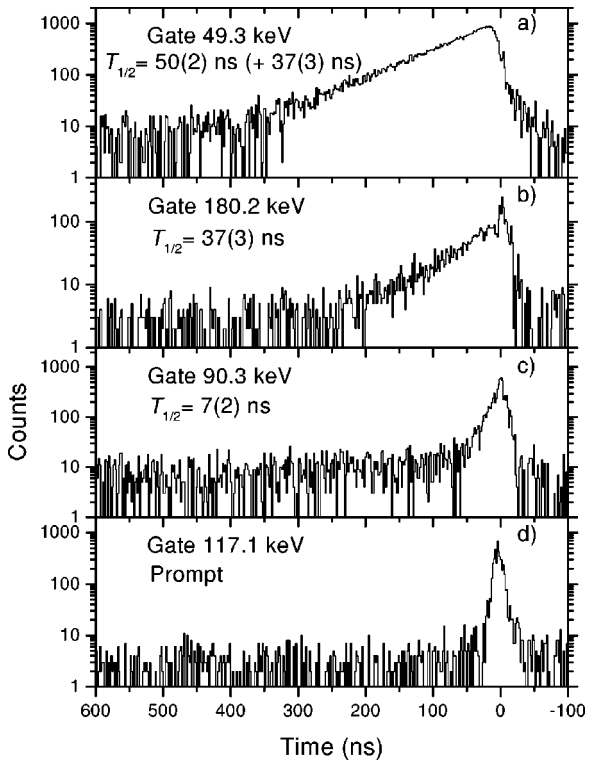

FIG. 7. Time spectra gated on (a) the 49.3 keV delayed transition (DT), (b) the 180.2 keV DT, (c) the 90.3 keV DT, and (d) the 117.1 keV prompt transition. The fitted half-life values are indicated.

ments (see discussion) and from constraints imposed by the $E1$ character of the 49.3 keV line which comes from intensity balances (see Table II). From the decay of ^{172}Ta [18] we can restrict the spin and parity of the ground state (g.s.) of ^{172}Ta to $I^{\pi}_{g.s.}=2^-,3^{\pm},4^-$. From rotational arguments (see discussion) we identify the g.s. as being the lowest state of band J_f, i.e., $I^{\pi}_{g.s.}=3^+$. This band (the favored part of band J) is extended in the present work up to $31\hbar$ and the unfavored part (J_u), observed here for the first time, up to $16\hbar$. The $E2$ character of the transitions holds from intensity balances and DCO ratios. Two weak linking transitions, the 308.8 and 381.7 keV lines, fix the relative spins of the J_f and J_u bands. Band I, observed up to $21\hbar$, depopulates through two $E1$ transitions, the 90.3 and 93.2 keV lines (see Table II). These transitions have been reported by Meissner and co-workers [19] in the decay of ^{172}W as linking a 93 keV energy state to a 3 keV one and the ground state of ^{172}Ta, respectively, being the relative γ intensity of the two transitions very similar to that observed in this work. We propose that the 93.2 keV line links the bandheads of bands I and J_f. We have found no linking transitions between states of band K and other states of ^{172}Ta and hence the negative parity is assigned to this band only from rotational arguments.

III. DISCUSSION

The identification of proton and neutron orbitals involved in the rotational bands of ^{172}Ta was based on the coupling schemes proposed in Refs. [8–11]. The starting point is the construction of a zero-order level scheme (Table IV). For the doubly odd ^{172}Ta the zero-order bandhead energies were obtained adding the average experimental single-quasiparticle energies from neighboring odd nuclei, ^{171}Hf [20], ^{173}W [21], ^{171}Ta [14], and ^{173}Ta [15] and neglecting the residual interaction which can split the $K_{\pm}=|\Omega_p\pm\Omega_n|$ states according to

TABLE III. Experimental and theoretical internal conversion coefficients for isomeric transitions in ^{172}Ta and assigned multipolarities. Theoretical icc values were obtained using the HSSIC code from the National Nuclear Data Center, Brookhaven National Laboratory.

E_γ (keV)	Line	α^{expt}	$\alpha^{\text{theor}}(E1)$	$\alpha^{\text{theor}}(E2)$	$\alpha^{\text{theor}}(M1)$	$\alpha^{\text{theor}}(M2)$	Assigned multipolarity
113.5	L	0.57(17)	0.04	1.19	0.41	5.50	$M1$
180.2	K	0.42(10)	0.07	0.23	0.70	3.59	$M1-E2$
	L	0.04(3)	0.01	0.15	0.11	0.88	

TABLE IV. Zero-order level scheme of ^{172}Ta. Entries are $K_{\pm}=|\Omega_p \pm \Omega_n|$ values, zero-order energies in keV, and expected mixing ratios. Excitation energies correspond to the average of ^{171}Ta and ^{173}Ta for protons and to the average of ^{171}Hf and ^{173}W for neutrons. (The values corresponding to aligned proton and neutron intrinsic spins have been underlined.)

$\pi\Omega_p^{\pi}[Nn_3\Lambda]$ E_{π} (keV)	$\nu\Omega_n^{\pi}[Nn_3\Lambda]$ E_{ν} (keV)	$\nu 1/2^-[521]$ 11	$\nu 5/2^-[512]$ 25	$\nu 7/2^+[633]$ 43
$\pi 1/2^-[541]$ 0		0^+, $\underline{1}^+$ 11 $\delta\approx 0$	$\underline{2}^+$, 3^+ 25 $\delta<0$	$\underline{3}^-$, 4^- 43 $\delta<0$
$\pi 5/2^+[402]$ 0		$\underline{2}^-$, 3^- 11 $\delta>0$	0^-, $\underline{5}^-$ 25 $\delta>0$	1^+, $\underline{6}^+$ 43 $\delta>0$
$\pi 7/2^+[404]$ 20		3^-, $\underline{4}^-$ 31 $\delta>0$	$\underline{1}^-$, 6^- 45 $\delta<0$	$\underline{0}^+$, 7^+ 63
$\pi 9/2^-[514]$ 175		$\underline{4}^+$, 5^+ 186 $\delta>0$	2^+, $\underline{7}^+$ 200 $\delta>0$	1^-, $\underline{8}^-$ 218 $\delta>0$

TABLE V. Moments of inertia and alignments, calculated alignments ($i^{\rm calc}=i_n+i_p$), band-crossing frequencies, experimental and calculated deviations of the crossing frequencies with respect to the even-even core (g.s.b., ground state band of ^{170}Hf). The calculated deviations, $\delta\hbar\omega_c^{\rm calc}$, are obtained adding the deviations of the odd-N and odd-Z neighboring nuclei.

Nucleus	Band[a]	$J_0/\hbar^2$ (MeV^{-1})	$J_1/\hbar^4$ (MeV^{-3})	i ($\hbar$)	$i^{\rm calc}$ ($\hbar$)	$\hbar\omega_c$ (MeV)	$\delta\hbar\omega_c$ (MeV)	$\delta\hbar\omega_c^{\rm calc}$ (MeV)
^{170}Hf	g.s.b.	29.0	208.3			0.270(5)		
^{171}Hf	$1/2^-[521]^{\rm fav}$	38.6	264.7	0.42		0.220(5)	-0.050	
	$1/2^-[521]^{\rm unf}$			-0.27				
	$5/2^-[512]$	32.5	249.5	0.31		>0.240	>-0.030	
	$7/2^+[633]$	41.5	26.5	1.78		0.350(10)	0.080	
^{171}Ta	$1/2^-[541]$	37.3	67.3	2.23		0.295(5)	0.025	
	$5/2^+[402]$	23.3	335.5	0.45		0.250(10)	-0.020	
	$7/2^+[404]$	25.8	372.1	0.52		0.270(15)	0.000	
	$9/2^-[514]$	28.1	257.4	0.94		0.265(5)	-0.005	
^{172}Ta	A$=\pi 1/2^-[541]\otimes\nu 7/2^+[633]$	44.6	23.8	3.77	4.01	>0.350	>0.080	0.105
	B$=\pi 9/2^-[514]\otimes\nu 7/2^+[633]$	45.0	41.3	2.48	2.72	0.340(5)	0.070	0.075
	E[b]$=\pi 9/2^-[514]\otimes\nu 5/2^-[512]$	31.6	298.6		1.25	>0.205	>-0.065	>-0.035
	F$=\pi 9/2^-[514]\otimes\nu 1/2^-[521]$	38.6	27.4	1.38	1.36	0.195(15)	-0.075	-0.055
	G$=\pi 7/2^+[404]\otimes\nu 7/2^+[633]$	48.4	18.2	1.06	2.30	0.290(10)	0.020	0.080
	H$=\pi 5/2^+[402]\otimes\nu 7/2^+[633]$	45.4	39.0	1.90	2.23	0.315(5)	0.045	0.060
	I$=\pi 7/2^+[404]\otimes\nu 1/2^-[521]$	44.5	81.9	1.07	0.94	0.245(5)	-0.025	-0.050
	I$=\pi 5/2^+[402]\otimes\nu 1/2^-[521]$	40.8	111.2	0.60	0.87	0.255(5)	-0.015	-0.070
	J_f[c]$=\pi 1/2^-[541]\otimes\nu 1/2^-[521]$	42.5	170.7	2.69	2.65	0.240	-0.030	-0.025
	$J_u=\pi 1/2^-[541]\otimes\nu 1/2^-[521]$			2.07	1.96			

[a]For ^{172}Ta we indicate the configuration (or the possible configurations) assigned.
[b]Moments of inertia correspond to calculated values ($J_{0,1}^{\rm calc}=J_{0,1p}+J_{0,1n}-J_{0,1core}$).
[c]Crossing frequency estimated from dynamical moments of inertia.

TABLE VI. Parameters used in the calculations of $B(M1)$ values. The alignments were extracted from ^{171}Ta and ^{171}Hf for the proton and neutron orbitals, respectively. The expectation values $\langle s_3 \rangle$ were calculated using Nilsson wave functions (see text).

	Protons				Neutrons		
Orbital	$i(\hbar)$	$\langle s_3 \rangle$	g_Ω	Orbital	$i(\hbar)$	$\langle s_3 \rangle$	g_Ω
$\pi 1/2^-[541]$	2.23	−0.023	0.87	$\nu 1/2^-[521]$	0.42	−0.167	0.90
$\pi 5/2^+[402]$	0.45	0.487	1.57	$\nu 5/2^-[512]$	0.31	0.319	−0.34
$\pi 7/2^+[404]$	0.52	−0.445	0.63	$\nu 7/2^+[633]$	1.78	0.343	−0.26
$\pi 9/2^-[514]$	0.94	0.450	1.29				

the Gallagher-Moszkowski coupling rules [22]. This zero-order set of bandhead energies most likely provides a complete level scheme for ^{172}Ta up to 300 keV. In order to identify the proton and neutron orbitals involved in a given rotational band we performed an analysis of band properties such as rotational alignments, band crossing frequencies, $B(M1)/B(E2)$ values, mixing ratios of $M1(E2)$ transitions, signature splitting, etc. The theoretical estimates of the $B(M1)/B(E2)$ ratios were obtained from the semiclassical formula of the cranking model developed by Dönau and Frauendorf [23] (see also Ref. [24]). In this context we used the following expressions:

$$B(M1, I \to I-1) = \frac{3}{8\pi}\mu_T^2$$

and

$$B(E2, I \to I-2) = \frac{5}{16\pi}\langle IK20|I-2K\rangle^2 Q_0^2,$$

where μ_T is the transverse magnetic moment given by

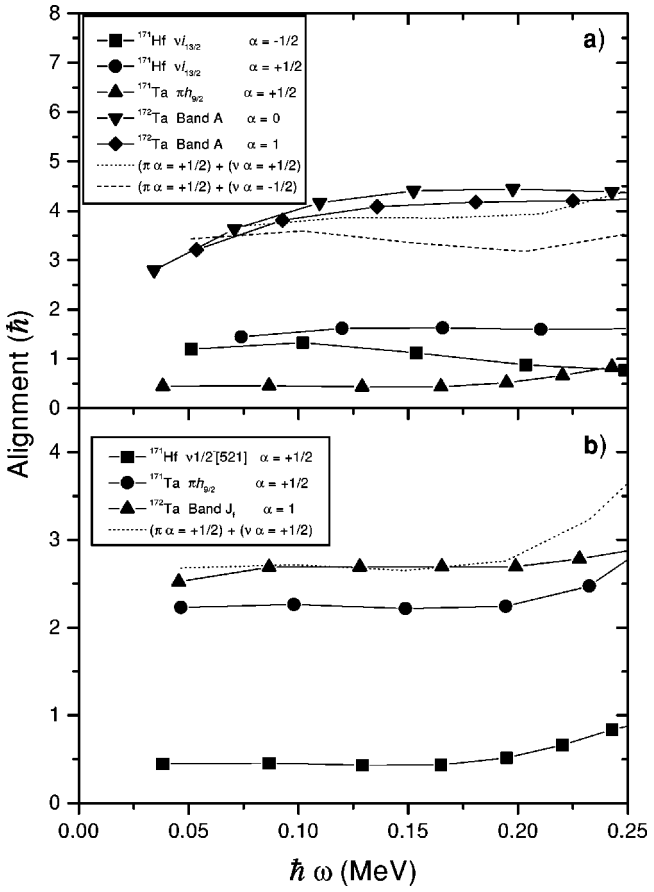

FIG. 8. Experimental alignments as a function of the rotational frequency corresponding to (a) band A and (b) band J_f. The values for the involved single-nucleon bands in neighboring odd-A nuclei are also plotted. Dotted and dashed lines correspond to the sum of these values.

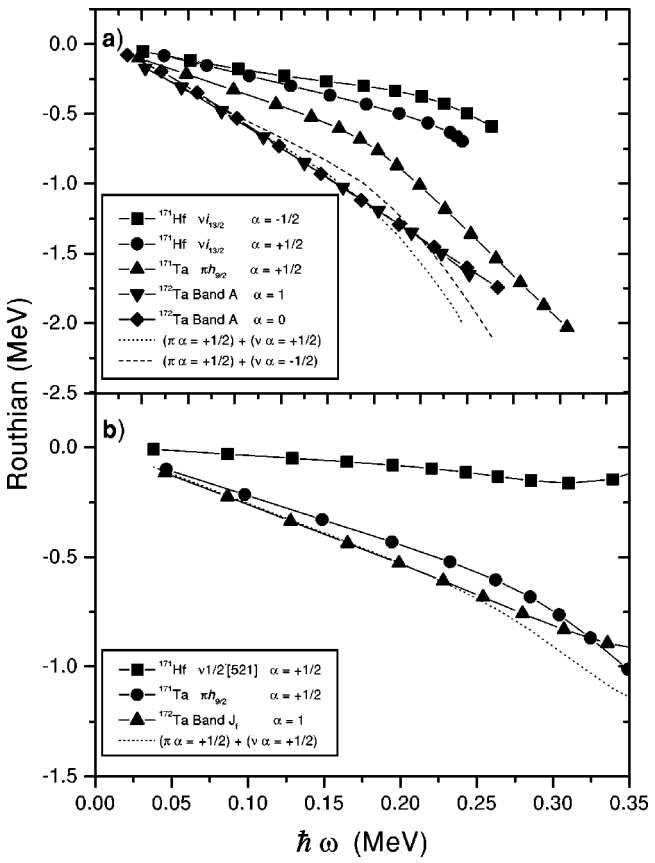

FIG. 9. Experimental Routhians as a function of the rotational frequency corresponding to (a) band A and (b) band J_f. The values for the involved single-nucleon bands in neighboring odd-A nuclei are also plotted. Dotted and dashed lines correspond to the sum of these values.

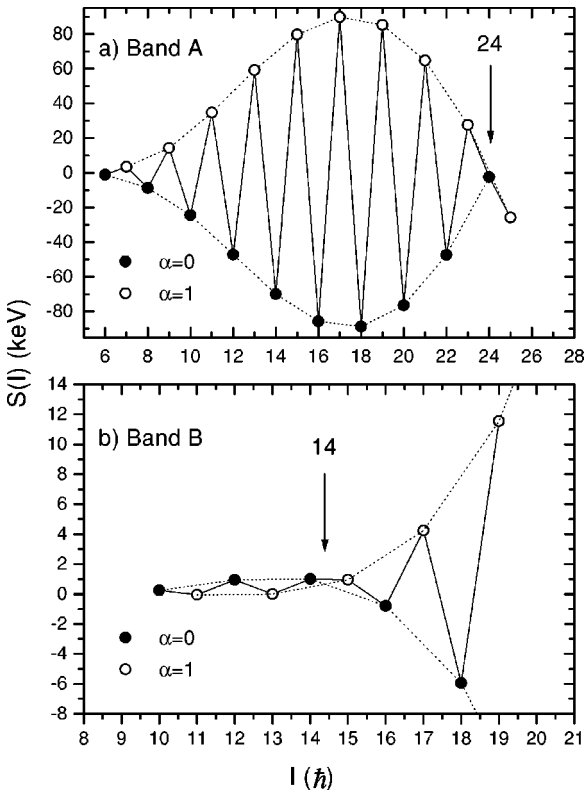

FIG. 10. Variation of the energy difference $S(I)=E(I)-E(I-1)-[E(I+1)-E(I)+E(I-1)-E(I-2)]/2$ between levels of (a) band A and (b) band B of ^{172}Ta, as a function of the angular momentum. The signature inversion point is indicated with an arrow.

$$\mu_T=(g_{\Omega_p}-g_R)(\Omega_p\sqrt{1-K^2/I^2}-i_pK/I)+(g_{\Omega_n}-g_R)\times(\Omega_n\sqrt{1-K^2/I^2}-i_nK/I),$$

g_{Ω_p}, g_{Ω_n}, and $g_R=0.3$ are the proton, neutron, and collective gyromagnetic factors, respectively. The quantities i_p and i_n represent the aligned angular momenta of the proton and the neutron, respectively. μ_T is in units of μ_N. The intrinsic quadrupole moment Q_0 was estimated from the half-life $T_{1/2}$ of the first 2^+ state of ^{170,2}Hf [25,26] to be 7.29 *e* b.

The mixing ratio δ for $\Delta I=1$ in-band transitions was evaluated using the expression

$$\delta=0.93E_\gamma Q_0K\sqrt{I^2-K^2}/(\mu_TI^2),$$

where E_γ is the transition energy in MeV.

For each rotational band the moments of inertia , J_0 and J_1, were extracted fitting the level energies through a fourth order cranking formula:

$$E=\tfrac{1}{2}(J_0+\tfrac{3}{2}J_1\omega^2)\omega^2,$$

where the rotational frequencies ω are obtained from the third order equation:

$$R=I_x-i=\sqrt{(I+\tfrac{1}{2})^2-K^2}-i=(J_0+J_1\omega^2)\omega,$$

where R is the collective and i is the particle contribution (which is also set as a free parameter in the calculation) to the total aligned angular momentum I_x. Table V summarizes the results obtained using this procedure for the extracted moments of inertia together with the alignments, and crossing frequencies for rotational bands belonging to ^{170}Hf [25], ^{171}Hf [20], ^{171}Ta [14], and ^{172}Ta. In the case of odd nuclei we also included the deviation of the crossing frequencies with respect to the even-even core, $\delta\hbar\omega_c$, and, in the case of ^{172}Ta, the calculated alignment ($i^{\rm calc}=i_n+i_p$) and the calculated deviation of the crossing frequencies, $\delta\hbar\omega_c^{\rm calc}$. Proton and neutron *g*-factors (g_{Ω_p}, g_{Ω_n}) were calculated by the expression [27] $g_\Omega=g_l+(g_s-g_l)\langle s_3\rangle/\Omega$. The expectation values of the spin projection on the symmetry axis, $\langle s_3\rangle$, were evaluated using Nilsson type wave functions obtained from the diagonalization of the deformed harmonic oscillator with $\beta=0.27$, the parameters κ and μ were extracted from Ref. [27]. For the orbital and spin *g*-factors we used $g_{l,p}=1$; $g_{s,p}=3.91$, $g_{l,n}=0$, and $g_{s,n}=-2.68$. Alignments, $\langle s_3\rangle$ and *g*-factors for the proton and neutron intrinsic states used in the calculations are listed in Table VI.

A. Band A

The configuration proposed for this band is $\pi h_{9/2}$ ($1/2^-[541]$)$\otimes\nu i_{13/2}$ ($7/2^+[633]$) [12]. This kind of coupling (an $\Omega=1/2$ decoupled orbital with a high-*j* intruder orbital, strongly affected by the Coriolis force) corresponds to a staggered semidecoupled structure [11]. It begins with low energy highly converted transitions and displays a pronounced odd-even staggering reflecting the same phenomenon present in $i_{13/2}$ bands. The effective projection quantum number K [24] has a value $K_{\rm eff}=1.1$, which is too small except for a highly compressed structure. This high compression is due to strong Coriolis effects in both $\pi h_{9/2}$ and $\nu i_{13/2}$ orbitals [11]. The large alignment of this band, $i=3.77$, is consistent with the presence of the proposed orbitals (see Table V). Furthermore, a rather good additivity in the average alignments is observed, $i^{\rm calc}=i_n(^{171}{\rm Hf})+i_p(^{171}{\rm Ta})=4.01$, remaining approximately constant over a wide range of rotational frequencies [see Fig. 8(a)]. A similar effect is obtained for the Routhians relative to the core [Fig. 9(a)]. The assigned configuration is also supported by the delay in the first backbend. The experimental crossing frequency of this band has the largest value, $\hbar\omega_c>0.350$ MeV, among all bands in ^{172}Ta, being consistent with the blocking of both orbitals (see Table V). Recently, signature inversion in this structure has been observed in ^{162,164}Tm, ^{174}Ta, and ^{176}Re [4–6]. In Fig. 10(a) we have plotted the quantity $S(I)=E(I)-E(I-1)-[E(I+1)-E(I)+E(I-1)-E(I-2)]/2$ vs I for this band. The signature inversion point is observed in this work at $I=24\,\hbar$ in agreement with systematics [6]. Below this point, states with odd spin, corresponding to the coupling between the favored signatures in both nucleons ($\alpha_p^f+\alpha_n^f=1/2+1/2=1$), are anomalously unfavored. In this context we assign an even spin to the first observed state of the band. In Fig. 11(a) we can see that calculated $B(M1)/B(E2)$ values

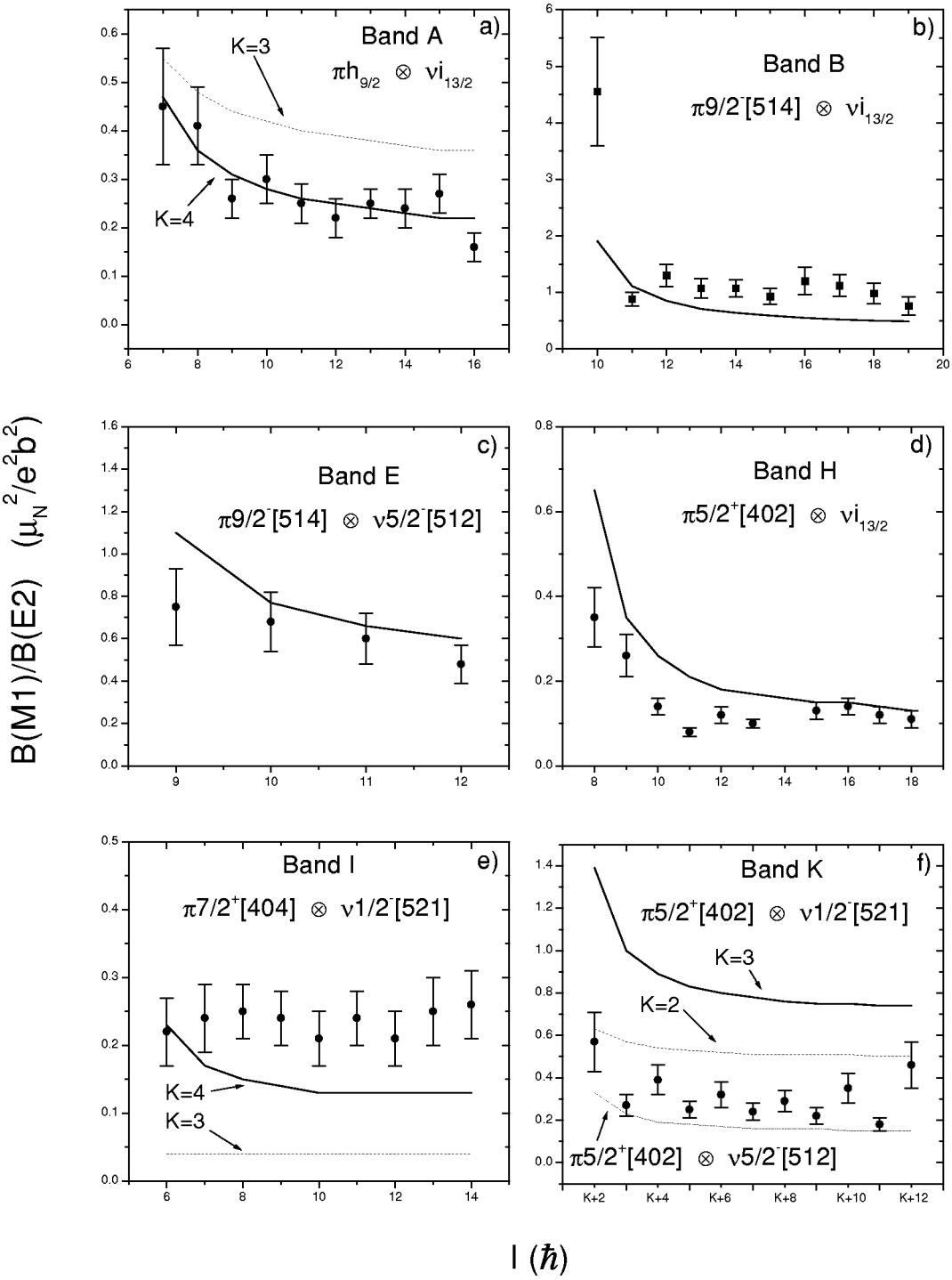

FIG. 11. Experimental and calculated $B(M1)/B(E2)$ values corresponding to (a) band A, (b) band B, (c) band E, (d) band H, (e) band I, and (f) band K of ^{172}Ta.

($K=3,4=7/2\mp1/2$ have been used because of the expected strong mixing due to the Coriolis interaction) fit very well the experimental values. Finally, the experimental DCO ratios for the $\Delta I=1$ in-band transitions indicate negative mixing ratios, as expected. A value $\delta_{\rm exp}=-0.30(5)$ is extracted from the 169.5 keV $(11^-)\rightarrow(10^-)$ transition [see Fig. 12(a)] while a calculated value $\delta=-0.23$ is obtained in the framework of the cranking model.

B. Band B

The configuration proposed for this band is $\pi h_{11/2}(9/2^-[514])\otimes\nu i_{13/2}(7/2^+[633])$. In this case we have the coupling between a normal orbital ($\pi h_{11/2}$) and a strongly Coriolis distorted orbital ($\nu i_{13/2}$) leading to a compressed structure [11]. The first $\Delta I=1$ transition is much smaller that the second one compared to the situation in a high-K normal band [$I(I+1)$ law]. We obtain a $K_{\rm eff}=3.3$

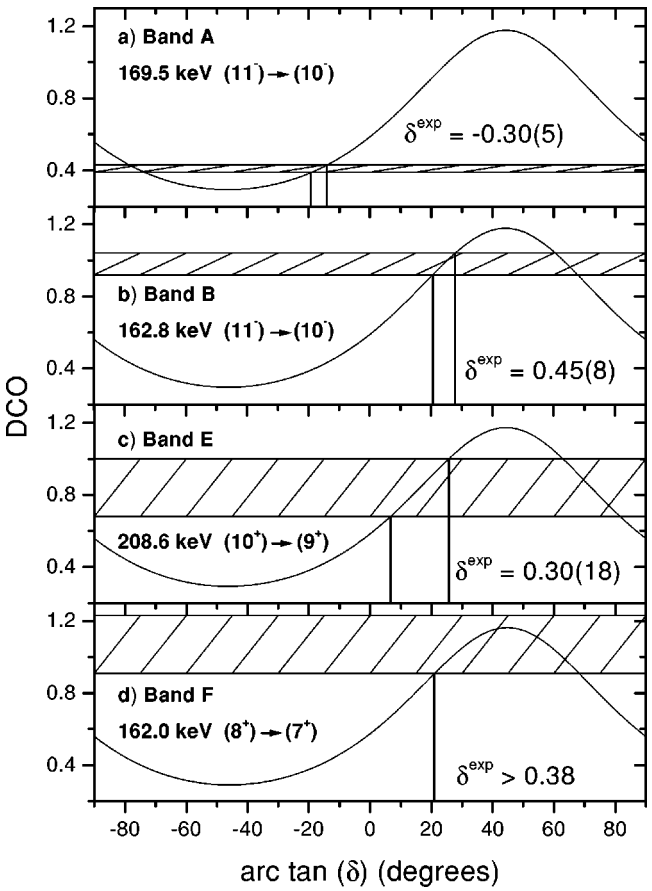

FIG. 12. Experimental and calculated DCO ratios for selected transitions of (a) band A, (b) band B, (c) band E, and (d) band F. The experimental mixing ratios are also indicated.

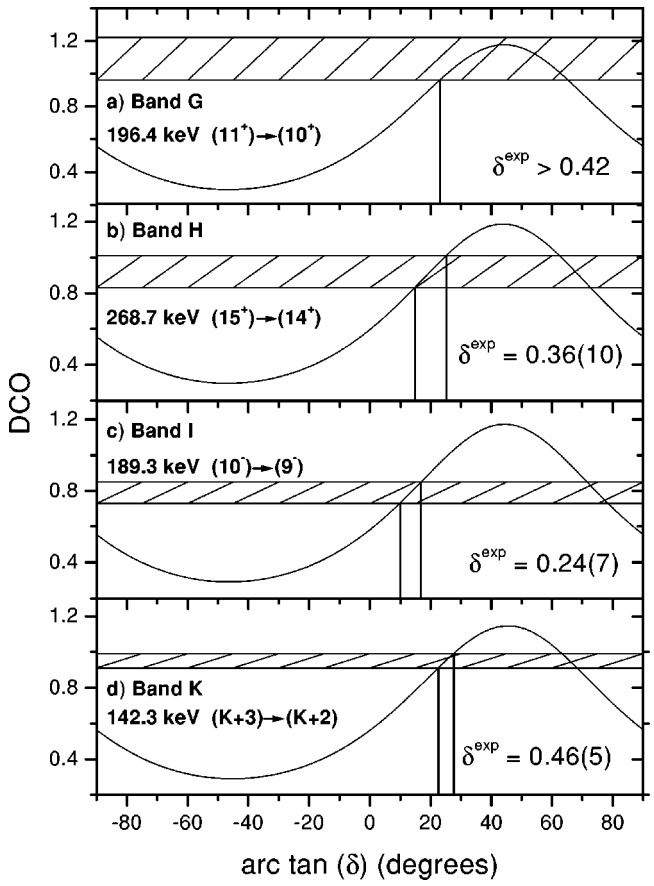

FIG. 13. Experimental and calculated DCO ratios for selected transitions of (a) band G, (b) band H, (c) band I, and (d) band K. The experimental mixing ratios are also indicated.

which reflects this compression if compared with $K=8$. From an experimental point of view, the linking to band A through $M1$ transitions fixes the negative parity of the band and limits the bandhead spin to 6, 7, or 8 $\hbar$. In Table IV we can see that the only other configuration that fulfills these conditions is the $\pi 7/2^+[404]\otimes\nu 5/2^-[512]$, $K^\pi=6^-$ band, but the coupling between two normal orbitals leads to a normal band with an expected $K_{\rm eff}\approx K$. The configuration assignment is also supported by the observed signature inversion [see Fig. 10(b)] characterizing this structure and observed in most nuclei of the rare-earth region (see Ref. [6] and references therein). The spin at which this inversion occurs, $I=14\hbar$, agrees with systematics (see Fig. 13 of Ref. [6]). The occupation of the $\nu i_{13/2}$ orbital is suggested, in the same way as in band A, by a delay in the crossing frequency if compared to the $\pi h_{11/2}$ band in ^{171}Ta. Good additivity effects are observed in the deviations of the crossing frequency ($\delta\hbar\omega_c=0.070$ MeV vs $\delta\hbar\omega_c^{\rm calc}=0.075$ MeV), and in the alignments ($i=2.48\hbar$ vs $i^{\rm calc}=2.72\hbar$). Experimental and calculated $B(M1)/B(E2)$ values for this band are observed in good agreement in Fig. 11(b). In addition, the experimental mixing ratios confirm the assignment. As an example we obtain from the 162.8 keV $(11^-)\rightarrow(10^-)$ transition [see Fig. 12(b)] $\delta_{\rm exp}=0.45(8)$ in agreement with the expected value $\delta=0.33$. This positive δ value also excludes the $\pi 7/2^+[404]\otimes\nu 5/2^-[512]$ configuration (see Table IV).

C. Bands C and D

Bands C and D can be interpreted as four-quasiparticle bands. Due to the uncertainties in spins and parities we are not able to unambiguously identify their configurations.

D. Band E

For this band we propose the configuration $\pi h_{11/2}(9/2^-[514])\otimes\nu 5/2^-[512]$. Both orbitals are weakly affected by the Coriolis interaction and the resulting coupling leads to a normal band [11]. In this case $K_{\rm eff}=7.5\approx K=7$. With the moment of inertia obtained from the first dipole transition of the band we obtain a value of 191.5 keV for the second transition, being the experimental one 190.5 keV. Cranking calculations result in bad fits for this band and no accurate values for moments of inertia and crossing frequency were obtained. Nevertheless, using calculated moments of inertia (see Table V), a lower limit for the crossing frequency has been extracted. The configuration assignment is also confirmed by the agreement between experimental and calculated $B(M1)/B(E2)$ values [Fig. 11(c)] and DCO ratios. The experimental mixing ratio corresponding to the 208.6 keV $(10^+)\rightarrow(9^+)$ transition [Fig. 12(c)] is $\delta_{\rm exp}=0.30(18)$ while the calculated one is $\delta=0.46$. The hindrance factor with respect to the Weisskopf estimate corresponding to the 25 keV transition, linking bands B and E is $F_W^{E1}\approx 2\times 10^4$.

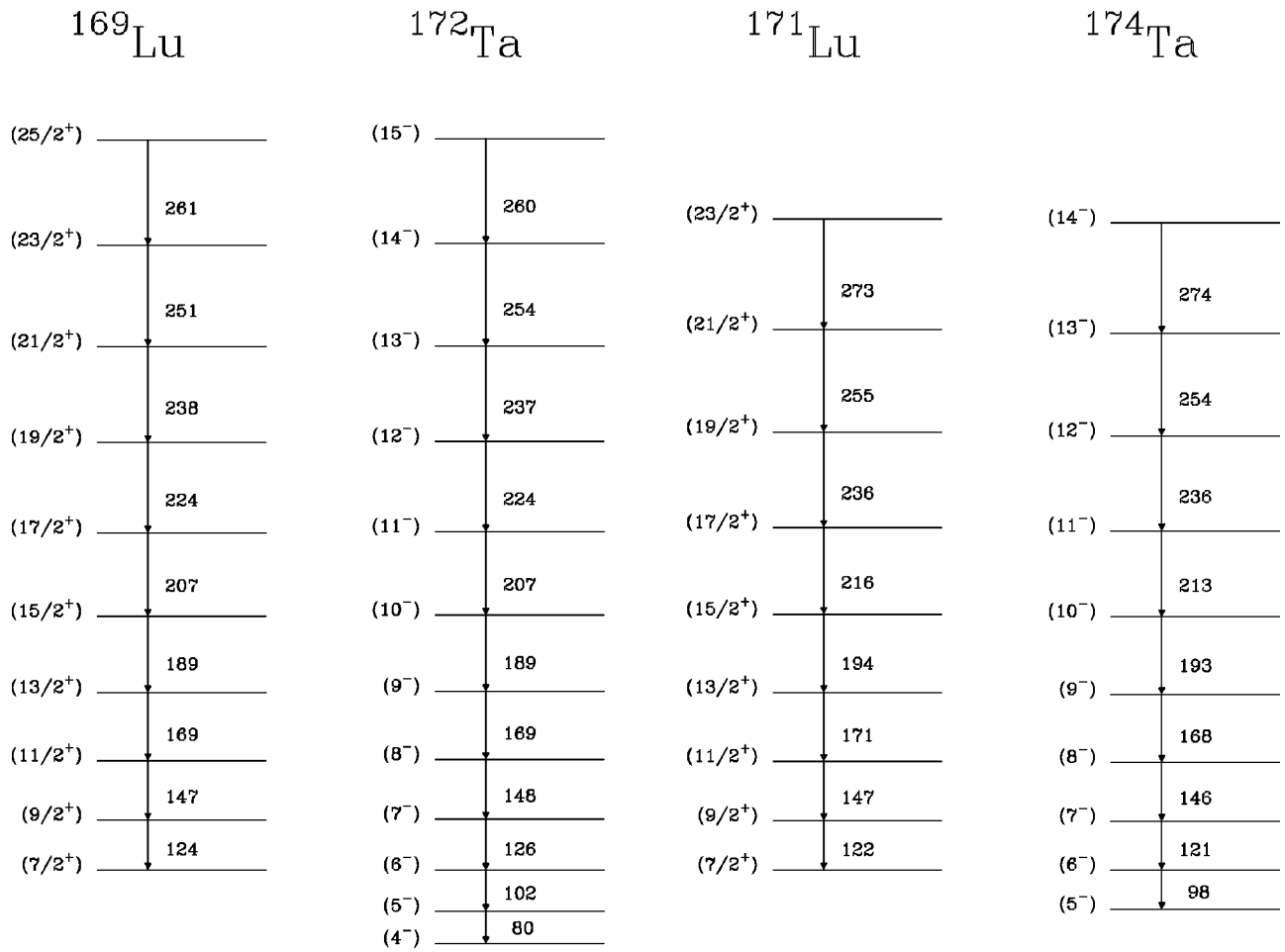

FIG. 14. Systematics of twin bands. The configuration assignments are ^{169}Lu: $\pi 7/2^+[404]$ (Ref. [29]), ^{172}Ta: $\pi 7/2^+[404] \otimes \nu 1/2^-[521]$ (this work), ^{171}Lu: $\pi 7/2^+[404]$ (Ref. [30]), and ^{174}Ta: $\pi 5/2^+[402] \otimes \nu 5/2^-[512]$ (Ref. [5]). Only partial $\Delta I=1$ cascades are drawn.

This value falls within the systematics [28] for a $\Delta K=0$ or 1 transition and, hence, the configuration assignment of band E is consistent with the corresponding one of band B.

E. Band F

The semidecoupled nonstaggered structure [11] $\pi h_{11/2}(9/2^-[514]) \otimes \nu 1/2^-[521]$ is proposed for this band. Experimentally, the bandhead can have spin from 5 to 9 $\hbar$ and the parity must be positive. The other possibilities for the configuration assignment correspond to $\pi 7/2^+[404] \otimes \nu i_{13/2}(7/2^+[633])$ and $\pi 5/2^+[402] \otimes \nu i_{13/2}(7/2^+[633])$, with $K=7,6$, respectively, but, for rotational arguments (see below), these structures are assigned to bands G and H. Band F and band B (the same proton orbital is occupied) look very similar, but there are some differences related to the neutron orbital involved. In band F, in contrast to band B, the backbending is not delayed. Moreover, this band has the smallest crossing frequency (see Table V) of all bands in this nucleus, reflecting the same feature of the band $\nu 1/2^-[521]$ in ^{171}Hf. The additivity of the deviations of the crossing frequencies and alignments is very good, $\delta\hbar\omega_c=-0.075$ MeV vs $\delta\hbar\omega_c^{\rm calc}=-0.055$ MeV and $i=1.38$ vs $i^{\rm calc}=i_n(^{171}{\rm Hf})+i_p(^{171}{\rm Ta})=1.36$. In this case, the compression due to the $\nu i_{13/2}$ orbital in band B is clearly not present, obtaining $K_{\rm eff}=4.9$ vs $K=5$. Due to the weakness of the band, no accurate branching ratios were obtained, nevertheless the DCO ratio corresponding to the 162.0 keV $(8^+)\rightarrow(7^+)$ transition [Fig. 12(d)] indicates a positive mixing ratio, $\delta_{\rm exp}>0.38$, in agreement with the expected value $\delta=0.18$.

F. Bands G and H

As mentioned above, the configurations proposed for bands G and H are $\pi 7/2^+[404] \otimes \nu i_{13/2}(7/2^+[633])$ and $\pi 5/2^+[402] \otimes \nu i_{13/2}(7/2^+[633])$, with $K=7,6$, respectively. The relative spins are fixed by the linking transitions and the bandhead spin of band G is greater in one unit than the corresponding to band H. These are new examples of compressed bands (see band B) due to the $\nu i_{13/2}$ orbital, its presence in both bands is suggested by the delay in the crossing frequency (see Table V). The effective projection quantum numbers are $K_{\rm eff}=3.5$ and 1.2, respectively, much smaller than the K values, $K=7,6$. Due to special cancellations in the calculation of the transverse magnetic moment in band G ($\mu_T\approx 0$ for $I=9,10$), the expected mixing ratios have large

values but undetermined signs. These large values are indicated by the experimental DCO ratios for this band which have values close to 1 [see Table I and Fig. 13(a)]. This fact prevents us from comparing experimental and calculated $B(M1)/B(E2)$ values. At variance with band G, band H does not present cancellations in the transverse magnetic moments, and the experimental and calculated $B(M1)/B(E2)$ values are in good agreement [see Fig. 11(d)]. The same is true for the mixing ratio, obtaining, for the 268.7 keV $(15^+)\rightarrow(14^+)$ transition [see Fig. 13(b)], $\delta_{\rm exp}=0.36(10)$ with an expected value $\delta=0.54$. The bandhead of band H depopulates through an $E1$, 49.3 keV, transition to a state with spin restricted to $I=5$, 6, or 7 $\hbar$ and negative parity. The only possible configurations (see zero order level scheme, Table IV) for this state are $\pi 5/2^+[402]\otimes\nu 5/2^-[512]$ and $\pi 7/2^+[404]\otimes\nu 5/2^-[512]$, with $K^\pi=5^-,6^-$, respectively. Moreover, these intrinsic states lie, at zero order, very close to the bandhead of band $\pi h_{9/2}(1/2^-[541])\otimes\nu i_{13/2}$ (band A) in agreement with the experiment. In addition, the hindrance factor with respect to the Weisskopf estimate corresponding to the 49.3 keV transition ($F_W^{E1}\approx 4\times 10^4$) falls within the systematics [28] for a $\Delta K=0$ or 1 transition. The rotational band corresponding to this intrinsic state is not observed. This is possible due to the fact that the gain in spin for normal bands is lower than for other kinds of bands, like compressed ones, and even at low spins they do not lie close to the yrast line.

G. Band I

Since band I has positive mixing ratios [see Fig. 13(c)], only three configurations (see Table IV) remain to be assigned to this band: (a) $\pi 7/2^+[404]\otimes\nu 1/2^-[521]$, $K^\pi=4^-$; (b) $\pi 5/2^+[402]\otimes\nu 1/2^-[521]$, $K^\pi=3^-$; (c) $\pi 5/2^+[402]\otimes\nu 5/2^-[512]$, $K^\pi=5^-$.

As mentioned before, the decay of ^{172}Ta [18] restricts the spin and parity of the ground state (g.s.) of ^{172}Ta to $I^\pi_{\rm g.s.}=2^-,3^\pm,4^-$, and band I depopulates to the g.s. through a 93.2 keV $E1$ transition. In this context, the g.s. of ^{172}Ta must be $I^\pi=3^+$, and the lowest state of band I, $I^\pi=3^-$ or 4^-, excluding configuration (c). The hindrance factor with respect to the Weisskopf estimate corresponding to the 93.2 keV transition is $F_W^{E1}\approx 1\times 10^5$, falling within the systematics [28] for a $\Delta K=0$ or 1 transition. The two remaining configurations (semidecoupled nonstaggered), (a) and (b) involve the neutron orbital $\nu 1/2^-[521]$, and the crossing frequency is expected to be smaller than the corresponding one of the core. The calculated deviations of the crossing frequency for these configurations ($\delta\hbar\omega_c^{\rm calc}=-0.050$ and -0.070 MeV, respectively), are consistent with the experimental values ($\delta\hbar\omega_c=-0.025$ and -0.015 MeV) (see Table V). The calculated alignments $i^{\rm calc}=0.94$, 0.87, corresponding to configurations (a) and (b) are also consistent with the experimental ones, $i=1.07$, 0.60, respectively. Experimental $B(M1)/B(E2)$ ratios are better reproduced by configuration (a) than (b), but the agreement seems to be not sufficient [see Figs. 11(e), and 11(f)]. In addition, we prefer the assignment $\pi 7/2^+[404]\otimes\nu 1/2^-[521]$, due to the fact that this band exhibits transition energies very similar to the band $\pi 7/2^+[404]$ in ^{169}Lu [29]. Figure 14 shows the $\Delta I=1$ cascades of $\pi 7/2^+[404]$ bands in ^{169,171}Lu [29,30], and our proposed $\pi 7/2^+[404]\otimes\nu 1/2^-[521]$ bands in ^{172,174}Ta. It is worth noting that Bark and co-workers [5] have assigned another configuration ($\pi 5/2^+[402]\otimes\nu 5/2^-[512]$) to this band in ^{174}Ta, mainly based on $B(M1)/B(E2)$ values. As already discussed, in ^{172}Ta this configuration cannot be assigned to band I and the similarity showed in Fig. 14 is striking. The phenomenon of twin bands (very similar transition energies) or identical (very similar moments of inertia) has been previously discussed in the normal deformation regime [1–3] and in the superdeformed regime [31,32], in which twin bands are also identical. In the present case the configuration assignment corresponds to the situation described in Ref. [1] in which a normal proton orbital ($\pi 7/2^+[404]$) is coupled to a decoupled neutron orbital ($\nu 1/2^-[521]$) with decoupling parameter $a_n\approx 1$. There are, however, three main differences.

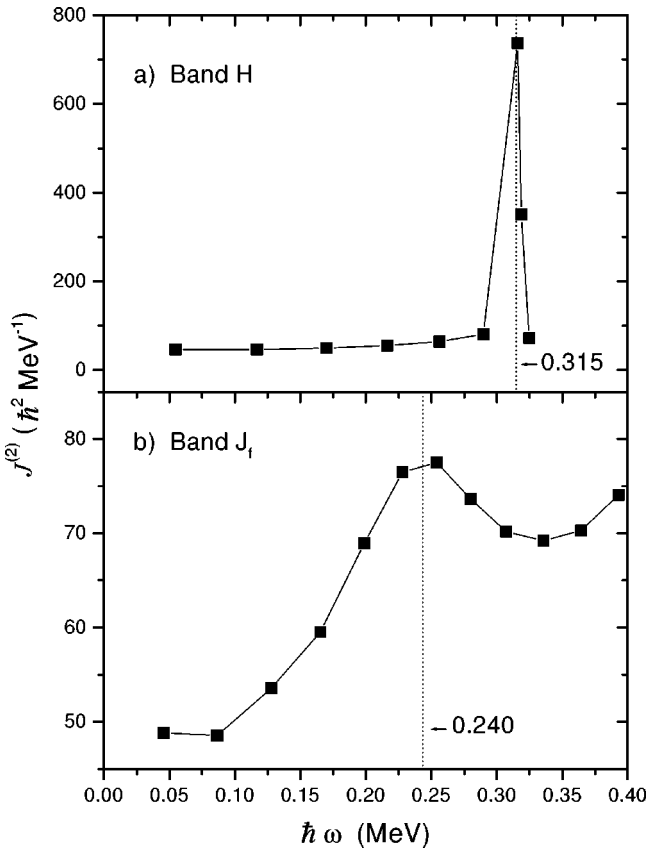

FIG. 15. Experimental dynamical moments of inertia as a function of the rotational frequency corresponding to (a) band H and (b) band J_f.

(1) Similar bands do not belong to the same element.

(2) The moments of inertia of the odd and doubly odd nuclei are different $J_0(^{169}{\rm Lu})=31.5\hbar^2\,{\rm MeV}^{-1}$, and $J_0(^{172}{\rm Ta})=44.5\hbar^2\,{\rm MeV}^{-1}$.

(3) Spins involved in similar transitions are not related as $I_{\text{odd-odd}}=I_{\rm odd}\pm 1/2$.

Accidental cancellations would be invoked as in Ref. [2] but the phenomenon is not yet well understood.

H. Bands J_f and J_u

Band J_f has been previously reported and discussed [12] and is interpreted as the favored part ($\alpha^f=\alpha_p^f+\alpha_n^f=1/2+1/2=1$) of the doubly decoupled band [11] $\pi h_{9/2}(1/2^-[541])\otimes\nu 1/2^-[521]$. Band J_u corresponds to the unfavored part of this structure ($\alpha^u=\alpha_p^f+\alpha_n^u=1/2-1/2=0$). $B(M1)$ values are expected to be very small, and only two weak dipole transitions are observed. Band J_f displays worth noting additivity effects. In Figs. 8(b) and 9(b) we plot the alignments and the Routhians relative to the core of band J_f in ^{172}Ta, band $\pi h_{9/2}$ in ^{171}Ta, and band $\nu 1/2^-[521]$ in ^{171}Hf. The sum of values corresponding to the odd-nuclei is also plotted in each figure resulting in curves fitting very well the alignment and routhian curves of band J_f, in a wide rage of rotational frequency. The alignment of band J_u is reduced because of the antialigned neutron (see Table V). The crossing frequency has been estimated from the dynamical moments of inertia due to the fact that the moments of inertia extracted from the first transitions in the cranking calculations are inadequate for the zone beyond the backbending. Figure 15 shows dynamical moments of inertia of bands H and J_f. The crossing frequency of band H obtained here agrees with the value obtained from the routhian (see Table V), and, then, the estimated value of band J_f is $\hbar\omega_c=0.240$ MeV. This value clearly indicates a compensation effect between the opposite trends due to the proton and neutron orbitals (see Table V).

I. Band K

No linking transitions have been observed between this band and any other band or state of this nucleus. DCO ratios for the $\Delta I=1$ transitions of this band are around 1 implying positive sign for δ [see Fig. 13(d)]. Two possibilities remain for this band: (a) $\pi 5/2^+[402]\otimes\nu 1/2^-[521]$, $K^\pi=3^-$ and (b) $\pi 5/2^+[402]\otimes\nu 5/2^-[512]$, $K^\pi=5^-$, both implying negative parity. No information about moments of inertia, alignments, and crossing frequencies are available for this band due to very bad fits obtained in cranking calculations. Nevertheless, the backbending seems to occur at a rotational frequency value less than the corresponding one to the core, in agreement with both configurations. $B(M1)/B(E2)$ values are plotted in Fig. 11(f), in which configuration (b) fits better than (a), but this is insufficient to discriminate between them.

IV. SUMMARY AND CONCLUSIONS

High-spin states in doubly odd ^{172}Ta were investigated by means of in-beam γ-ray spectroscopy techniques using the multidetector array GASP at Legnaro, Italy, and the low energy facility at Buenos Aires, Argentina. Eleven rotational bands have been observed and their configurations discussed. In this context, coupling schemes have revealed as a correct tool to assign configurations to the observed structures. Twin bands in the normal deformation regime have been found, but the mechanism to produce these bands is still an open subject.

[1] A. J. Kreiner, Phys. Rev. C **38**, R2486 (1988).

[2] D. Hojman, A. J. Kreiner, and M. Davidson, Phys. Rev. C **46**, 1203 (1992).

[3] G. Levinton, A. J. Kreiner, M. A. Cardona, M. E. Debray, D. Hojman, J. Davidson, G. Martí, A. Burlón, M. Davidson, D. R. Napoli, M. De Poli, D. Bazzacco, N. Blasi, S. M. Lenzi, G. Lo Bianco, C. Rossi Alvarez, and V. R. Vanin, Phys. Rev. C **60**, 044309 (1999).

[4] R. A. Bark, J. M. Espino, W. Reviol, P. B. Semmes, H. Carlsson, I. G. Bearden, G. B. Hagemann, H. J. Jensen, I. Ragnarsson, L. L. Riedinger, H. Ryde, and P. O. Tjøm, Phys. Lett. B **406**, 193 (1997).

[5] R. A. Bark, H. Carlsson, S. J. Freeman, G. B. Hagemann, F. Ingebretsen, H. J. Jensen, T. Lönnroth, M. J. Piiparinen, I. Ragnarsson, H. Ryde, H. Schnack-Petersen, P. B. Semmes, and P. O. Tjøm, Nucl. Phys. **A630**, 603 (1998).

[6] M. A. Cardona, A. J. Kreiner, D. Hojman, G. Levinton, M. E. Debray, M. Davidson, J. Davidson, R. Pirchio, H. Somacal, D. R. Napoli, D. Bazzacco, N. Blasi, R. Burch, D. De Acuña, S. M. Lenzi, G. Lo Bianco, J. Rico, and C. Rossi Alvarez, Phys. Rev. C **59**, 1298 (1999).

[7] J. P. Schiffer and W. W. True, Rev. Mod. Phys. **48**, 191 (1976).

[8] A. J. Kreiner, M. Fenzl, S. Lunardi, and M. A. J. Mariscotti, Nucl. Phys. **A282**, 243 (1977).

[9] A. J. Kreiner, J. Davidson, M. Davidson, D. Abriola, C. Pomar, and P. Thieberger, Phys. Rev. C **36**, 2309 (1987); **37**, 1338 (1988).

[10] A. J. Kreiner, in *Proceedings of the International Conference on Contemporary Topics in Nuclear Structure Physics, Cocoyoc, Mexico, 1988*, edited by R. F. Casten, A. Frank, M. Moshinsky, and S. Pittel (World Scientific, Singapore, 1988), p. 521, and references therein.

[11] A. J. Kreiner, in *Proceedings of the XII Workshop on Nuclear Physics, Cataratas del Iguazú, Argentina, 1989*, edited by M. C. Cambiaggio, A. J. Kreiner, and E. Ventura (World Scientific, Singapore, 1989), p. 137.

[12] A. J. Kreiner, D. Hojman, J. Davidson, M. Davidson, M. Debray, G. Falcone, D. Santos, C. W. Beausang, D. B. Fossan, R. Ma, E. S. Paul, S. Shi, and N. Xu, Phys. Lett. B **215**, 629 (1988).

[13] D. Bazzacco, in Proceedings of the International Conference on Nuclear Structure at High Angular Momentum, Ottawa, 1992 [Report No. AECL 10613 (unpublished)], Vol. 2, p. 376.

[14] J. C. Bacelar, R. Chapman, J. R. Leslie, J. C. Lisle, J. N. Mo, E. Paul, A. Simcock, J. C. Willmott, J. D. Garrett, G. B. Hagemann, B. Herskind, A. Holm, and P. M. Walker, Nucl. Phys. **A442**, 547 (1985).

[15] H. Carlsson, R. A. Bark, L. P. Ekström, A. Nordlund, H. Ryde, G. B. Hagemann, S. J. Freeman, H. J. Jensen, T. Lönnroth, M. J. Piiparinen, H. Schnack-Petersen, F. Ingebretsen, and P. O. Tjøm, Nucl. Phys. **A592**, 89 (1995).

[16] I. Kurniawan, T. Aoki, T. Komatsubara, T. Hosoda, and M. Yamanouchi, Nucl. Phys. **A534**, 367 (1991).

[17] D. R. Tilley, H. R. Weller, C. M. Cheves, and R. M. Chasteler, Nucl. Phys. **A595**, 1 (1995).

[18] M. H. Cardoso, P. F. A. Goudsmit, and J. Konijn, Nucl. Phys. **A205**, 121 (1973).
[19] F. Meissner, W.-D. Schmidt-Ott, V. Freystein, T. Hild, E. Runte, H. Salewski, and R. Michaelsen, Z. Phys. A **337**, 45 (1990).
[20] V. S. Shirley, Nucl. Data Sheets **66**, 69 (1992).
[21] V. S. Shirley, Nucl. Data Sheets **75**, 377 (1995).
[22] C. J. Gallagher, Jr. and S. A. Moszkowski, Phys. Rev. **111**, 1282 (1958).
[23] F. Dönau and S. Frauendorf, in *Proceedings of the Conference on High Angular Momentum Properties of Nuclei, Oak Ridge, TN, 1982*, edited by N. Johnson (Harwood Academic, Chur, Switzerland, 1982), p. 143.
[24] D. Hojman, A. J. Kreiner, M. Davidson, J. Davidson, M. Debray, E. W. Cybulska, P. Pascholati, and W. A. Seale, Phys. Rev. C **45**, 90 (1992).
[25] C. M. Baglin, Nucl. Data Sheets **77**, 125 (1996).
[26] B. Singh, Nucl. Data Sheets **75**, 199 (1995).
[27] A. Bohr and B. Mottelson, *Nuclear Structure* (Benjamin, Reading, MA, 1975), Vol. 2.
[28] K. E. G. Löbner, in *The Electromagnetic Interaction in Nuclear Spectroscopy*, edited by W. D. Hamilton (North-Holland, Amsterdam, 1975), p. 141.
[29] C. Foin, D. Barnéoud, S. A. Hjorth, and R. Berthoux, Nucl. Phys. **A199**, 129 (1973).
[30] P. Kemnitz, L. Funke, K.-H. Kaun, H. Sodan, G. Winter, and M.I. Baznat, Nucl. Phys. **A209**, 271 (1973).
[31] T. Byrski, F. A. Beck, D. Curien, C. Schuck, P. Fallon, A. Alderson, I. Ali, M. A. Bentley, A. M. Bruce, P. D. Forsyth, D. Howe, J. W. Roberts, J. F. Sharpey-Schafer, G. Smith, and P. J. Twin, Phys. Rev. Lett. **64**, 1650 (1990).
[32] W. Nazarewicz, P. J. Twin, P. Fallon, and J. D. Garret, Phys. Rev. Lett. **64**, 1654 (1990).